Actin Depolymerization Disrupts Tight Junctions via Caveolae-mediated Endocytosis◻

Le Shen and Jerrold R. Turner

Department of Pathology, The University of Chicago, Chicago, IL 60637

The tight junction (TJ) determines epithelial barrier function. Actin depolymerization disrupts TJ structure and barrier function, but the mechanisms of this effect remain poorly understood. The goal of this study was to define these mechanisms. Madin-Darby canine kidney (MDCK) cells expressing enhanced green fluorescent protein-, enhanced yellow fluorescent protein-, or monomeric red fluorescent protein 1-fusion proteins of β-actin, occludin, claudin-1, ZO-1, clathrin light chain A1, and caveolin-1 were imaged by time-lapse multidimensional fluorescence microscopy with simultaneous measurement of transepithelial electrical resistance (TER). Actin depolymerization was induced with latrunculin A (LatA). Within minutes of LatA addition TER began to fall. This coincided with occludin redistribution and internalization. In contrast, ZO-1 and claudin-1 redistribution occurred well after maximal TER loss. Occludin internalization and TER loss, but not actin depolymerization, were blocked at 14°C, suggesting that membrane traffic is required for both events. Inhibition of membrane traffic with 0.4 M sucrose also blocked occludin internalization and TER loss. Internalized occludin colocalized with caveolin-1 and dynamin II, but not with clathrin, and internalization was blocked by dominant negative dynamin II (K44A), but not by Eps15Δ95-295 expression. Inhibition of caveolae-mediated endocytosis by cholesterol extraction prevented both LatA-induced TER loss and occludin internalization. Thus, LatA-induced actin depolymerization causes TJ structural and functional disruption by mechanisms that include caveolae-mediated endocytosis of TJ components.

INTRODUCTION

A primary function of epithelia is to create a barrier that separates distinct tissue compartments. This barrier is formed by the plasma membranes of individual epithelial cells and the tight junction (TJ), which seals the space between adjacent cells. TJ proteins include the claudin family of transmembrane proteins (Furuse *et al.*, 1998; Colegio *et al.*, 2003), other transmembrane proteins, including occludin and junctional adhesion molecules (Furuse *et al.*, 1993; Martin-Padura *et al.*, 1998), and cytoplasmic plaque proteins such as ZO-1, ZO-2, ZO-3, and cingulin (Stevenson *et al.*, 1986; Citi *et al.*, 1988; Jesaitis and Goodenough, 1994; Haskins *et al.*, 1998). The claudin family of proteins dictates the charge selective permeability of the TJ (Simon *et al.*, 1999; Colegio *et al.*, 2003). In contrast, the specific function of most other TJ protein remains ill-defined. However, studies of cultured cells and genetically modified mice show that additional proteins, including ZO-1 and occludin, are important for proper epithelial function (McCarthy *et al.*, 1996;

Abbreviations used: BS^3, bis(sulfosuccinimidyl)suberate; EGFP, enhanced green fluorescent protein; HBSS, Hank's balanced saline solution; LatA, latrunculin A; MBCD, methyl-β-cyclodextrin; MDCK, Madin-Darby canine kidney; mRFP1, monomeric red fluorescent protein 1; TER, transepithelial resistance; TJ, tight junction.

Chen *et al.*, 1997; Wittchen *et al.*, 1999; Bazzoni *et al.*, 2000; Nusrat *et al.*, 2000a; Ryeom *et al.*, 2000; Saitou *et al.*, 2000; Bruewer *et al.*, 2004; Umeda *et al.*, 2004).

In addition to specific TJ proteins, a ring of filamentous actin encircles each epithelial cell at the level of the apical junctional complex and physically interacts with the TJ (Madara, 1987). The functional dependence of the TJ barrier on this perijunctional actomyosin ring was first recognized 25 years ago when it was shown that pharmacological disruption of this ring disrupts barrier function (Bentzel *et al.*, 1980). This cytoskeletal and TJ disruption is associated with retraction of microfilaments from the plasma membrane, altered cell shape, local accumulations of condensed actin (Meza *et al.*, 1982), disruption of the parallel strands that comprise the TJ as seen by freeze-fracture electron microscopy (Madara *et al.*, 1986), and redistribution of the TJ plaque protein ZO-1 (Madara *et al.*, 1986; Stevenson and Begg, 1994). Because ZO-1 and the transmembrane protein occludin bind directly to actin filaments, most have concluded that the effects of actin depolymerization on TJ structure and function are secondary to loss of these binding interactions with subsequent disruption of molecular TJ structure. However, no data demonstrate this proposed mechanism to be accurate. Moreover, whereas pharmacological actin disruption induces rapid loss of barrier function, the described morphological changes occur more slowly. Thus, we concluded that identification and characterization of specific morphological changes that are temporally correlated with loss of barrier function might provide important new insights into the mechanisms by which this simple model stimulus, actin depolymerization, disrupts TJ function.

We expressed fluorescent fusion proteins of β-actin, occludin, claudin-1, ZO-1, clathrin light chain A1, and caveo-

lin-1 in epithelial monolayers. These were imaged using a new apparatus that allows simultaneous measurement of epithelial barrier function and fluorescence microscopy. Although most previously described morphological changes induced by actin depolymerization occurred well after barrier function loss was complete, we noted that vesicular removal of occludin from the TJ correlated well with loss of barrier function. Inhibition of this internalization prevented TJ barrier function loss after actin depolymerization. The data show that actin depolymerization causes TJ disruption by inducing caveolae-mediated endocytosis of TJ components that include occludin.

MATERIALS AND METHODS

Reagents

Latrunculin A (LatA); Alexa Fluor 488-conjugated phalloidin; Alexa Fluor 350-, 488-, or 594-conjugated secondary antibodies; rabbit anti-green fluorescent protein (GFP) antibody; and Hoechst 33342 were from Molecular Probes (Eugene, OR). Mouse monoclonal anti-occludin, rabbit anti-claudin-1, mouse anti-ZO-1, and mouse anti-claudin-4 antibodies were from Zymed Laboratories (South San Francisco, CA). Rabbit anti-caveolin-1 antibodies were from Abcam (Cambridge, MA) and Santa Cruz Biotechnology (Santa Cruz, CA). Rabbit anti-clathrin heavy chain antibodies also were from Santa Cruz Biotechnology. Rabbit anti-dynamin II was from Calbiochem (San Diego, CA). Rabbit anti-EEA1 was from Affinity Bioreagents (Golden, CO). Rat anti-lysosome-associated membrane protein (LAMP)-1 monoclonal antibody (clone ID4B) was the generous gift of Dr. M. R. Clark (The University of Chicago, Chicago, IL). Rat anti-E-cadherin (clone DECMA-1), chlorpramazine, amiloride, filipin III, methyl-β-cyclodextrin, and water-soluble cholesterol were all from Sigma (St. Louis, MO). LY294002 was from Cell Signaling Technology (Beverly, MA). All other chemicals were of the highest grade available.

Plasmids

The enhanced green fluorescent protein (EGFP)-β-actin construct was generated by fusing EGFP (BD Biosciences Clontech, Palo Alto, CA) to the amino terminus of human β-actin (I.M.A.G.E. clone 769559; American Type Culture Collection, Manassas, VA) and cloning the construct into pcDNA6/TR (Invitrogen, Carlsbad, CA). Monomeric red fluorescent protein 1 (mRFP1), a gift from Roger Y. Tsien and Robert E. Campbell (University of California, San Diego, La Jolla, CA) (Campbell et al., 2002), was cloned into NheI-KpnI sites of pcDNA3.1 zeo (+) (Invitrogen) to form the pmRFP1-C vector. mRFP1-tagged occludin was generated by PCR amplification and cloning of the coding region of human occludin, a gift from Randall J. Mrsny (Cardiff University, Cardiff, United Kingdom) into KpnI-XbaI sites of pmRFP1-C vector in frame with mRFP1. mRFP1-ZO-1 was generated using the coding region of pSK-ZO-1, a kind gift from Alan S. Fanning and James M. Anderson (University of North Carolina, Chapel Hill, NC) by first inserting KpnI sites flanking the coding region and then cloning the coding region into the KpnI site of pmRFP1-C. EGFP-claudin-1 was generated by PCR amplification of coding region of human claudin-1 (I.M.A.G.E. clone 4500534; American Type Culture Collection) and cloning into the KpnI-XbaI sites of pEGFP-C1 (BD Biosciences Clontech). Integrity of the plasmids was verified by restriction digestion and direct sequencing of the expression construct and adjacent regions. Dynamin II-EGFP, dyamin II-K44A-EGFP, EGFP-dynamin I, and EGFP-dynamin I-K44E (Di et al., 2003) were graciously provided by Dr. H. C. Palfrey (The University of Chicago). Caveolin-1-EGFP and enhanced yellow fluorescent protein (EYFP)-clathrin light chain A1 (Massol et al., 2004) were kindly provided by Dr. T. Kirchhausen (Harvard Medical School and the CBR Institute for Biomedical Research, Boston, MA). EGFP-Eps15Δ95-295 (Nichols et al., 2001) was generously provided by Dr. J. Lippincott-Schwartz (National Institutes of Health, Bethesda, MD).

Cell Culture and Transfection

Madin-Darby canine kidney (MDCK) cells (American Type Culture Collection) were grown in DMEM with 1 g/l glucose (Mediatech, Herndon, VA) supplemented with 10% fetal bovine serum (Invitrogen) and 15 mM HEPES, pH 7.4. For growth as monolayers cells were plated at confluent density, media were replenished at 24 h, and monolayers were studied 48 h after plating. Stable transfectants were generated by transfection with Lipofectamine 2000 (Invitrogen) in 100-mm dishes, as described previously (Zhao et al., 2004). After growth in medium supplemented with 2.5 mg/ml G418 (Mediatech) or 15 μg/ml blasticidin S (Calbiochem, San Diego, CA) for 2 wk, cells were trypsinized and sorted into 96-well plates using a MoFlow cell sorter (DakoCytomation California, Carpinteria, CA). After expansion, clones with readily-detectable TJ fluorescence were selected for further study. Monolayers of stable transfectants were cultured in media with 7.5 mM sodium butyrate to augment transgene expression, from 24 to 48 h after plating and then transferred to media without sodium butyrate for 4 h before use. Transiently-transfected MDCK cells were plated directly onto Transwells and studied 2 d after transfection.

LatA Treatment

Monolayers were equilibrated in Hank's balanced saline (HBSS) with 15 mM HEPES, pH 7.4, for 1 h at 37°C before study. The basolateral media were then exchanged for HBSS containing LatA. For studies at different temperatures, monolayers were equilibrated at indicated temperatures for 30 min (after equilibration in HBSS at 37°C) before LatA treatment. To synchronize vesicle formation and internalization monolayers were cooled to 14°C before and during 30 min of LatA treatment to allow actin depolymerization. The temperature was then raised to 37°C to allow synchronous endocytosis.

Inhibitor Studies

For inhibitor studies, monolayers were transferred to HBSS as described above. Appropriate inhibitors were added bilaterally and monolayers incubated for 1 h at 37°C before basolateral LatA addition. For cholesterol depletion/repletion experiments monolayers were treated with methyl-β-cyclodextrin (MBCD) for 45 min followed by transfer to media containing MBCD or 1:10 cholesterol–MBCD complexes (Christian et al., 1997) for an additional 45 min. Monolayers were then treated with LatA as described above.

Transepithelial Electrical Resistance (TER) Measurement

TER was measured using electrodes placed on either side of the monolayer. These were attached to a current clamp (University of Iowa Bioengineering, Iowa City, IA) or EVOM (WPI, Saratosa, FL), as described previously (Turner et al., 1997; Wang et al., 2005).

Determination of F-Actin Content

Confluent MDCK monolayers were washed, equilibrated in HBSS for 1 h at 37°C, and transferred to HBSS at indicated temperatures for 30 min. Monolayers were then transferred to HBSS of the same temperature with LatA and fixed in 3% paraformaldehyde in HBSS at indicated times. After washing with HBSS with 50 mM NH$_4$Cl and permeabilization in HBSS containing 3% bovine serum albumin (BSA) and 0.5% saponin monolayers were incubated with 0.5 μM Alexa Fluor 488-conjugated phalloidin and 0.2 μg/ml Hoescht 33342 in HBSS with 3% BSA and 0.5% saponin for 1 h at room temperature. After five washes in HBSS with 3% BSA and 0.5% saponin and one wash with HBSS, fluorescent intensity was measured (Synergy HT; Bio-Tek Instruments, Winooski, VT). Alexa Fluor 488 fluorescence was normalized to Hoechst 33342 fluorescence to correct for cell number.

Immunofluorescence Staining

Monolayers were fixed with 1% paraformaldehyde in phosphate-buffered saline (PBS), pH 7.4, with 1 mM CaCl$_2$ for 30 min at room temperature. After three washes in PBS and a 15-min incubation in PBS with 50 mM NH$_4$Cl cells were permeablized in PBS with 3% BSA and 0.05% saponin. Monolayers were then incubated with primary antibody in PBS with 3% BSA and 0.05% saponin overnight at 4°C; washed five times with PBS, 3% BSA, and 0.05% saponin; and incubated with the appropriate Alexa Fluor 350-, 488-, or 594-conjugated secondary antibodies. After five washes monolayers were rinsed in water and mounted in SlowFade (Molecular Probes).

To retain intracellular vesicles, monolayers were briefly washed with ice-cold HBSS and fixed in methanol overnight at −20°C. After fixation monolayers were air-dried, rehydrated with 100 μM bis(sulfosuccinimidyl)suberate (BS^3) in PBS with 0.1% n-octyl-glutaraldehyde (PBS+) for 30 min, washed in PBS+, quenched in 100 mM ethylenediamine, pH 7.5, and washed once more in PBS+. Monolayers were then blocked in 1% nonfat dry milk, 1% fish gelatin, and 1% normal donkey serum in PBS+ for 1 h; incubated with primary antibodies for 2 h; washed; and incubated with the appropriate Alexa Fluor 350-, 488-, or 594-conjugated secondary antibodies for 1 h. After five washes, monolayers were rinsed in water and mounted in SlowFade.

Immunoblotting

MDCK monolayers prepared as described above were washed once with ice-cold HBSS and lysed directly in nonreducing SDS-PAGE sample buffer. After boiling at 95°C for 5 min, aliquots were resolved on SDS-PAGE gels (Bio-Rad, Hercules, CA) and transferred to polyvinylidene difluoride membranes. Membranes were blocked in 5% nonfat dry milk in Tris-buffered saline (TBS), washed in TBS with 0.05% Tween 20 (TBS-T), and incubated with primary antibodies in TBS with 1% nonfat dry milk overnight at room temperature. Membranes were washed with TBS-T, incubated with appropriate horseradish peroxidase-conjugated secondary antibodies (Cell Signaling Technology), and washed with TBS-T before detection by enhanced chemiluminescence (SuperSignal; Pierce Chemical, Rockford, IL).

Subcellular Fractionation

Monolayers were washed with 37°C HBSS and then scraped into ice-cold HBSS. After recovery by centrifugation at 4°C, cells were resuspended in TBS containing 1 mM 4-(2-aminoethyl)benzenesulfonyl fluoride, 0.8 mM aprotinin, 0.5 mM bestatin, 15 μM E-64, 20 μM leupeptin, and 10 μM pepstatin A and lysed by 60 passes through a bent 25-gauge needle. Cell disruption was monitored microscopically. Lysates (4 ml) were loaded above 8-ml 10–60% continuous sucrose gradients (in TBS) and centrifuged at 280,000 × g for 18 h at 4°C. Then, 0.5-ml fractions were collected and analyzed for sucrose concentration by refractometry and distribution of specific proteins by SDS-PAGE and immunoblot.

Fluorescence Microscopy with Simultaneous TER Measurement

Monolayers were mounted in a Petri dish in a custom-designed temperature-controlled stage (Brook Industries, Lake Villa, IL). TER was measured using an EVOM and Ag-AgCl electrodes embedded in the Petri dish base and fastened to the side of the microscope objective. Multidimensional imaging was performed by using an epifluorescence microscope (DMLB; Leica Microsystems, Bannockburn, IL), a 63× HCX PL APO L U-V-I aqueous immersion objective, and a 51022 filter set optimized for EGFP/mRFP1 (Chroma Technology, Rockingham, VT). The z-stacks were collected in 0.2–0.5 μm steps using motorized excitation filter wheels, z-motor, and shutter (Ludl, Hawthorne, NY) and a Retiga EXi camera (Q Imaging, Burnaby, British Columbia, Canada) controlled by MetaMorph 6 (Universal Imaging, Downingtown, PA).

For fixed cells, stained monolayers were observed using the same microscope equipped with an 88000 filter set (Chroma Technology) and 63× or 100× PL APO oil immersion objectives. The z-stacks were collected at 0.2-μm intervals. Image stacks were deconvolved using AutoDeblur 9.3 (Autoquant, Watervliet, NY).

Morphometric Analysis

Deconvolved z-stacks were merged, after pseudocolor assignment, using MetaMorph. Vesicles were defined as round or oval structures present in three or more z-planes. The number of vesicles in a single cell was counted over the full height of the cell. Signals were considered to be colocalized if there was ≥80% overlap between channels. For each measurement, 20 average-shaped and -sized cells chosen randomly were counted.

Statistical Analysis

All data are presented as average ± SE. All experiments were performed with triplicate or greater samples, and data shown are representative of three or more independent studies. P value was determined by two-tailed Student's t test and was considered to be significant if ≤0.05.

RESULTS

F-Actin Depolymerization Leads to Functional and Morphological TJ Disruption

Alteration of epithelial barrier function by cytochalasins is well established (Bentzel et al., 1980) and has been reported to exhibit an unusual biphasic dose dependence: low doses cause mild increases in TER, whereas higher doses cause TER to fall (Stevenson and Begg, 1994; Turner, 2000) (Figure 1A). The mechanism of this biphasic response has not been defined, but it may reflect the multiple mechanisms by which cytochalasins disrupt actin filaments, because cytochalasins cap barbed ends at low doses, whereas at higher concentrations they also sever microfilaments (MacLean-Fletcher and Pollard, 1980; Cooper, 1987; Spector et al., 1989). We therefore compared the effects of cytochalasin D to those of LatA, which causes microfilament depolymerization by a single mechanism, binding to and sequestration of G-actin monomers (Spector et al., 1983; Morton et al., 2000). Like cytochalasin D, LatA caused TER to fall at 0.2 μM (Figure 1A). However, unlike cytochalasin D, low doses of LatA did not cause TER to increase. Because of this simpler monophasic TER response to LatA treatment, LatA was used throughout these studies aimed at defining the mechanisms by which actin depolymerization disrupts TJ structure and function. Kinetic analyses of the effects of LatA on TER and F-actin content showed that LatA reduced F-actin content by 17 ± 0.4% and TER by 17 ± 0.6% within 5 min (Figure 1B).

Both F-actin content and TER continued to decrease over time, falling by 42 ± 1.4 and 82 ± 1.1%, respectively, at 30 min. Thus, TER decreases induced by LatA correlated temporally with actin depolymerization.

To identify morphological changes in TJ and perijunctional actin structure that correlate with loss of barrier function, monolayers were fixed using standard paraformaldehyde protein cross-linking, and specific TJ proteins or F-actin was labeled (Figure 1, C–G). Unlike decreases in TER and F-actin content, morphological changes were not detected until at least 20 min after LatA addition, long after substantial TER loss had occurred. The morphological changes detected included disruption of perijunctional actin, with alternating actin-rich and actin-poor zones, loss of microvillus F-actin, formation of apical actin aggregates (Figure 1C), loss of basal stress fibers (Figure 1D), and disruption of TJ-localized occludin (Figure 1E), ZO-1 (Figure 1F), and claudin-4 (Figure 1G). Although consistent with previous reports of actin and ZO-1 redistribution after actin disruption by cytochalasin D, these data show that this approach only detects morphological changes well after LatA-induced barrier function loss has occurred.

Development and Characterization of Fluorescent TJ Fusion Proteins

The data mentioned above demonstrate that traditional immunofluorescence approaches are unsuitable for identification of specific morphological changes that correlate with LatA-induced loss of barrier function. We therefore developed fusion proteins of β-actin, occludin, ZO-1, and claudin-1 using two fluorochromes: EGFP and mRFP1 (Campbell et al., 2002). EGFP and mRFP1 fluoresce with high quantum yield at wavelengths that are resolvable from one another, thus allowing their use for double labeling. These fluorescent proteins were linked to the amino termini of β-actin and ZO-1 because similar constructs have been shown to be effective (Choidas et al., 1998; Riesen et al., 2002). For claudins, both amino and carboxy-terminus fusions constructs have been reported (Sasaki et al., 2003; Matsuda et al., 2004), but, because the carboxy terminus is required for interaction with PDZ domains, e.g., of ZO-1, the fusion protein was attached to the amino terminus of claudin-1. Similarly, occludin was tagged at the amino terminus, because the carboxy terminus has been reported to be important for interactions with other proteins (Nusrat et al., 2000a; Peng et al., 2003). These fusion proteins were stably expressed in green (EGFP)–red (mRFP1) pairs in MDCK monolayers. Compared with the corresponding endogenous protein, each transfected fusion protein represented no more than one-half of the total of that protein (Figure 2, A–C). Expression of β-actin, ZO-1, and claudin-1 fusion proteins did not alter TER of transfected MDCK monolayers (our unpublished data). Expression of occludin increased TER by 21 ± 4%. This effect was similar, but less pronounced, than that reported after expression of chicken occludin in MDCK monolayers (McCarthy et al., 1996), suggesting that the fusion construct is a functional occludin protein. All transfected lines were sensitive to LatA with dose-responses and kinetics similar to nontransfected MDCK monolayers (our unpublished data). Morphological analyses of the distributions of these proteins showed that, in each case, the tagged fusion protein colocalized completely with the endogenous protein (Figure 2, D–F), suggesting that the tagged proteins are correctly targeted. Subcellular fractionation studies provide further evidence for correct targeting of tagged proteins, because both mRFP1-occludin and EGFP-claudin-1 comigrated with endogenous proteins in subcellular frac-
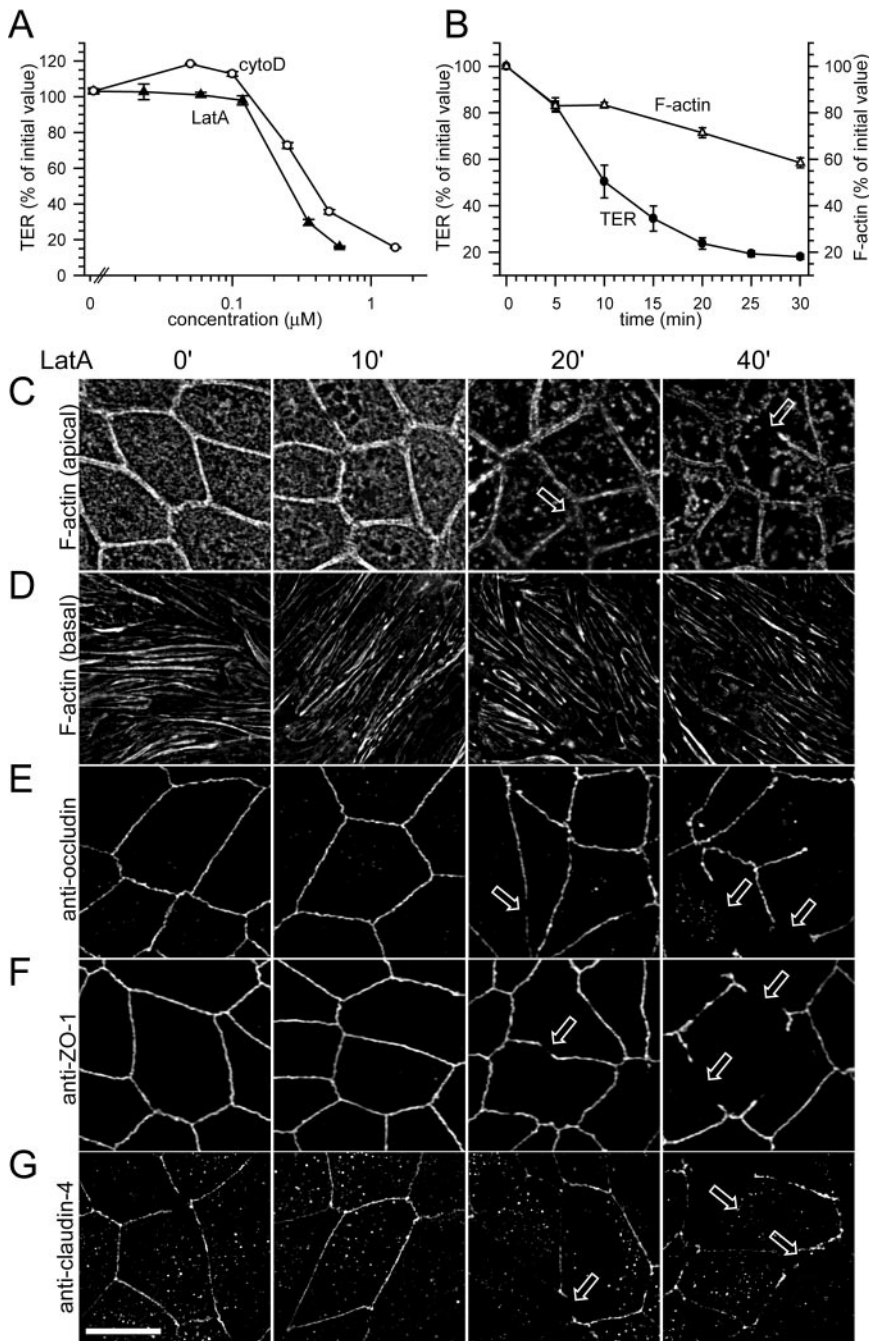
Figure 1. LatA-induces functional and structural TJ disruption. (A) MDCK monolayers were treated with indicated concentrations of LatA or cytochalasin D (cytoD). TER is shown 30 min after drug addition. Low doses of cytochalasin D increased TER, whereas higher doses reduced TER. LatA only caused dose-dependent TER loss. (B) TER loss parallels F-actin loss after LatA addition. Monolayers were treated with 0.5 μM LatA for indicated times. (C–G) LatA causes progressive disruption of F-actin and TJ proteins. Monolayers were treated with 0.5 μM LatA for indicated times, fixed, and stained with phalloidin to detect F-actin (C and D). Images at the level of the TJ (C) and basal stress fibers (D) are shown. Progressive loss of apical actin with partial fragmentation of the perijunctional actin ring (arrows) is apparent at 20 min. Basal stress fiber density also decreased beginning 20 min after LatA addition. LatA treatment induced discontinuities (arrows) in TJ distribution of occludin (E), ZO-1 (F), and claudin-4 (G) that were first detectable after 20 min. Bar, 10 μm.

tions in transfected cells and were of the same density as endogenous occludin or claudin-1 in nontransfected cells (Figure 2, G and H). Thus, the fusion proteins do not disrupt TJ assembly, LatA response, or targeting of endogenous TJ proteins and are themselves appropriately targeted, as assessed morphologically and biochemically. Therefore, these fusion proteins are suitable tools for analysis of TJ dynamics in live cells.

Live Cell Imaging Allows the Identification of Structural Changes That Are Temporally Correlated with LatA-induced Loss of Barrier Function

We analyzed polarized MDCK monolayers expressing fluorescent fusion proteins in an apparatus that allows simulta-

neous imaging and electrophysiological analysis (Figure 3A). Preliminary experiments showed that both protein localization and TER were generally stable during imaging of these monolayers, although subtle movements of individual TJ proteins within the TJ and minor cell shape changes could be detected (Figure 3B and Supplemental Movie S1). Thus, this apparatus is suitable for real-time analyses of TJ protein distribution and TER.

Distributions of fluorescent fusion proteins were initially imaged by collecting z-stacks at 1-min intervals before and after addition of LatA. TER was measured simultaneously. In monolayers expressing EGFP-β-actin and mRFP1-occludin, the latter was uniformly distributed along the TJ before LatA addition. Within 2 min after LatA addition, when TER
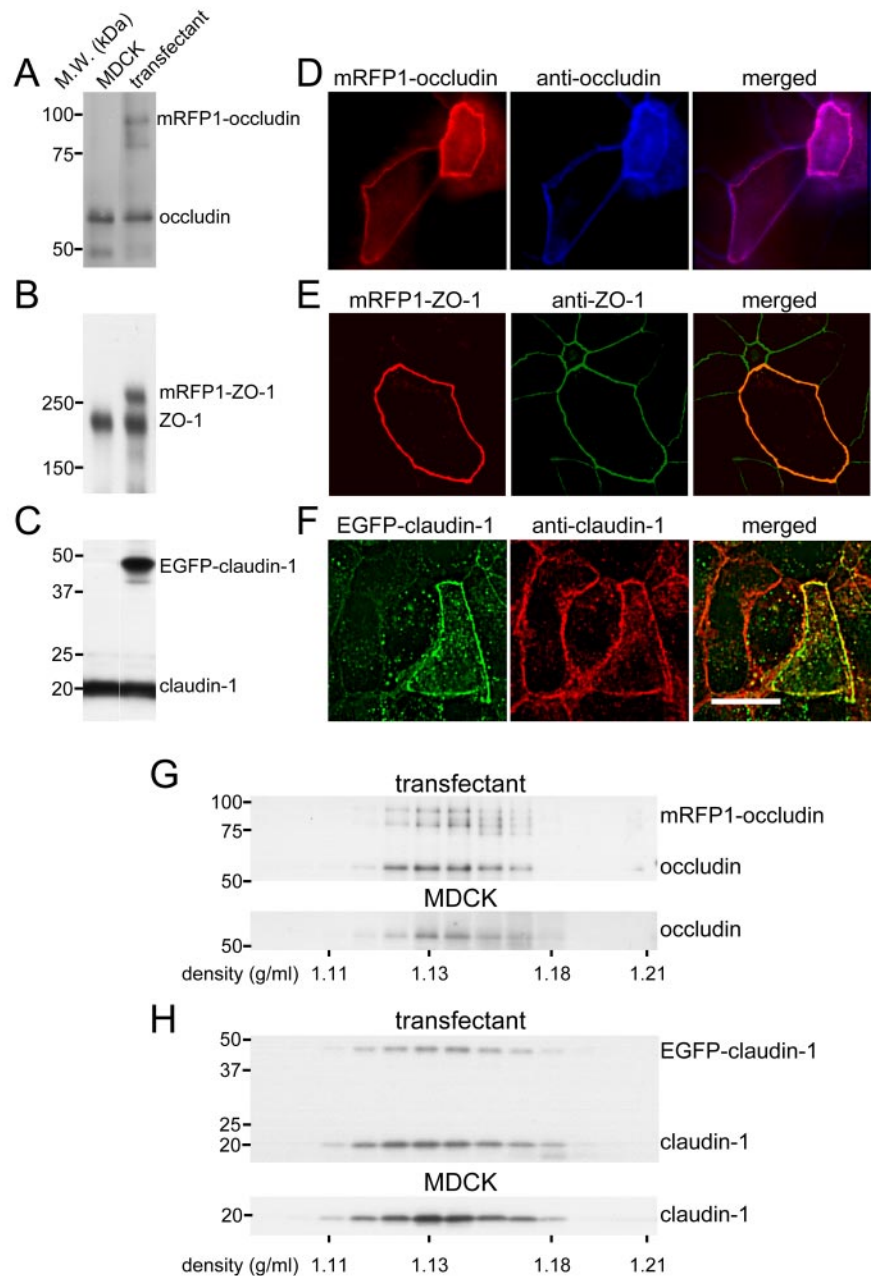
Figure 2. Expression of fluorescent tagged tight junction proteins in MDCK monolayers. (A–C) Lysates of nontransfected (MDCK) and stably transfected (transfectant) MDCK cells expressing mRFP1-occludin (A), mRFP-ZO-1 (B), and EGFP-claudin-1 (C) were studied by immunoblot. Fusion protein expression is less than or equal to endogenous expression for each protein. (D–F) Monolayers of stably-transfected MDCK cells expressing mRFP1-occludin (D), mRFP-ZO-1 (E), and EGFP-claudin-1 (F) were fixed and immunostained for the corresponding endogenous protein. Fusion proteins (left) colocalized with endogenous proteins (middle) in all cases. (G and H) Lysates of nontransfected (MDCK) and stably transfected (transfectant) monolayers expressing mRFP1-occludin (G) or EGFP-claudin-1 (H) were separated on isopycnic sucrose gradients. Fractions were analyzed by SDS-PAGE and immunoblot. Fusion proteins are found in the same fractions as endogenous proteins, both in stable transfectants and when compared with nontransfected cells.

decreases were first detected, distribution of mRFP1-occludin at the TJ became nonuniform, with alternating zones relatively enriched in or depleted of mRFP1-occludin (Figure 3C and Supplemental Movie S2). This persisted throughout the z-stack and was therefore not due to vertical redistribution or an artifact of imaging. EGFP-β-actin localization changed similarly and regions with decreased mRFP1-occludin generally also had reduced EGFP-β-actin fluorescence, suggesting a coordinated redistribution of EGFP-β-actin and mRFP1-occludin. The small zones enriched in mRFP1-occludin frequently formed small buds and then separated from the TJ in a process that was repeated frequently over the first 15 min after LatA addition (Figure 3D). To further characterize this process of occludin removal from the TJ, imaging was performed at higher rates. These images clearly show that occludin is first concentrated in a small zone within the TJ, followed by local invagination, rounding, and detach-

ment (Figure 3E and Supplemental Movie S3). These data are therefore consistent with endocytic removal of occludin after LatA addition. Analysis of xz reconstructions of fixed monolayers immunostained for occludin, as shown in Figure 3F, demonstrated budding and detached structures near the lower portion of the TJ, i.e., adjacent to the border of the TJ and lateral membrane, in LatA-treated monolayers. Occludin internalization continued as TER fell and was accompanied by progressive increases in numbers of intracellular occludin-containing vesicles. Loss of TER and mRFP1-occludin redistribution were accompanied by EGFP-β-actin reorganization, including appearance of EGFP-β-actin aggregates, and changes in cell shape (Figure 3C and Supplemental Movie S2). At later times after LatA addition, residual TJ-associated mRFP1-occludin was only present in dot like structures that also contained EGFP-β-actin. Thus, endocytic removal from the TJ is the primary morphological
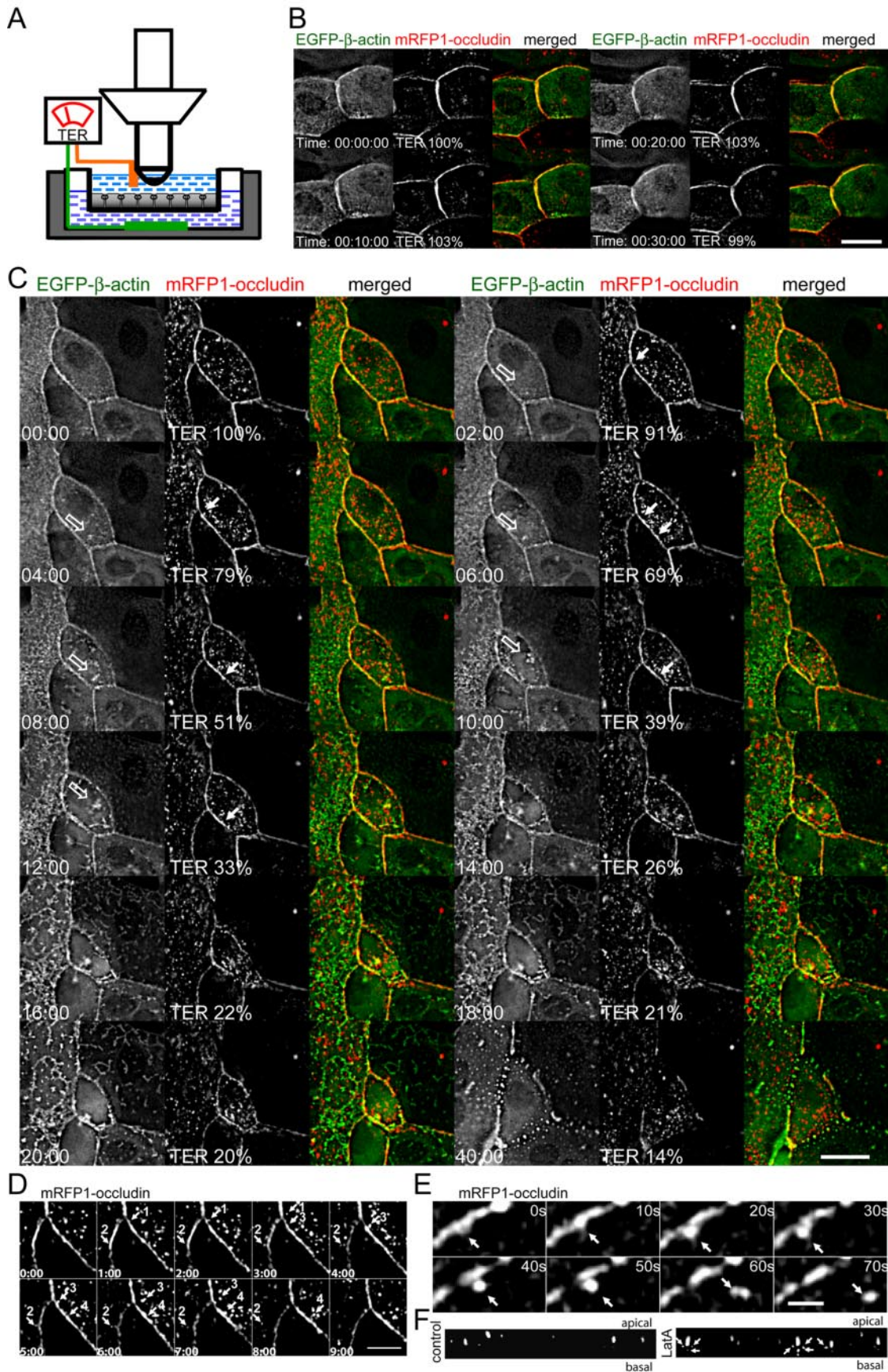
Figure 3.

change in occludin distribution that correlates with LatA-induced loss of barrier function.

Similar studies were performed using monolayers expressing EGFP-β-actin and mRFP1-ZO-1 (Figure 4A and Supplemental Movie S4). LatA-induced redistribution of EGFP-β-actin in these monolayers was similar to that in monolayers expressing EGFP-β-actin and mRFP1-occludin, thus providing an internal control for comparisons. Although mRFP1-ZO-1 fluorescent intensity did vary along the TJ during first 20 min after LatA addition, this variability was similar to that in control monolayers without LatA addition. As in the fixed immunostained preparations, significant mRFP1-ZO-1 redistribution was only detected >20 min after LatA addition, long after the majority of TER losses had occurred. At these times, mRFP1-ZO-1 was lost from large areas of the TJ. Like mRFP1-occludin, the mRFP1-ZO-1 that remained at the TJ colocalized with the EGFP-β-actin. However, in contrast to mRFP1-occludin, new intracellular pools of mRFP1-ZO-1 were not identified. Thus, the mRFP1-ZO-1 redistribution detected occurs after the bulk of TER loss and is not associated with occludin internalization.

The effect of LatA on claudin-1 distribution was studied using MDCK cells stably transfected with EGFP-claudin-1 and mRFP1-occludin (Figure 4B and Supplemental Movie S5). As in cells expressing EGFP-β-actin and mRFP1-occludin, LatA induced redistribution and internalization of mRFP1-occludin. In contrast, EGFP-claudin-1 was not re-

---

Figure 3 (facing page). Live cell imaging during LatA treatment allows identification of morphological events that correlate with TER loss. (A) Experimental apparatus. MDCK monolayers grown on 24-mm-diameter Transwells are mounted over a modified 35-mm-diameter culture dish in a temperature-controlled stage (set to 37°C unless noted otherwise). An aqueous immersion objective images the monolayer from the apical media. Ag-AgCl electrodes on both sides of the monolayer are linked to an EVOM to measure TER. (B) Confluent monolayers stably expressing EGFP-β-actin (left) and mRFP1-occludin (middle) were imaged as z-stacks at 1-min intervals for 30 min. As is typical for transgenes expressed in MDCK, fusion protein expression, i.e., fluorescent intensity, varies between cells. A single z-plane at the level of the TJ is shown. Both TER and localization of EGFP-β-actin and mRFP1-occludin were stable over this period. Bar, 20 μm. (C) Confluent monolayers stably expressing EGFP-β-actin (left) and mRFP1-occludin (middle) were imaged as z-stacks at 1-min intervals for 40 min after addition of 0.5 μM LatA. A single z-plane at the level of the TJ is shown. Time after LatA addition and TER, normalized to TER before LatA addition, are shown in each frame. Open arrows show aggregation and fusion of actin at the apical surface. Solid arrows show changes of mRFP1-occludin fluorescent intensity along the TJ and formation of mRFP1-occludin containing vesicles. Bar, 20 μm. (D) Confluent monolayers stably expressing mRFP1-occludin (shown) and EGFP-β-actin (not shown) were imaged as z-stacks at 1-min intervals for 40 min after addition of 0.5 μM LatA. A single z-plane at the level of the TJ is shown. Time after LatA addition is shown in each frame. Arrows show multiple vesicles emanating from the TJ beginning 2 min after LatA addition. Bar, 10 μm. (E) Confluent monolayers stably expressing mRFP1-occludin (shown) and EGFP-β-actin (not shown) were cooled to 14°C, treated with 0.5 μM LatA for 30 min, and warmed to 37°C. They were then imaged as limited z-stacks at 10-s intervals. A single z-plane at the level of the TJ is shown. Arrows show the process of occludin concentration, budding, and detachment to form a single vesicle. Bar, 2 μm. (F) Monolayers were treated as in E to synchronize vesicle budding. 10 min after warming to 37°C monolayers were fixed with −20°C methanol/BS³, stained for occludin, and z-stacks collected. Representative xz reconstructions of control and LatA-treated monolayers are shown. LatA treatment causes the appearance of budding and detached occludin-positive structures near the lower portion of the TJ, i.e., adjacent to the border of the TJ and lateral membrane.

---

moved from the TJ during the first 12 minutes after LatA addition. At later time points, the distribution of EGFP-claudin-1 became discontinuous at the TJ. At these times EGFP-claudin-1 at the TJ was present primarily in areas containing mRFP1-occludin. Although claudin internalization has been reported in steady-state epithelial monolayers (Matsuda *et al.*, 2004), in response to calcium depletion (Ivanov *et al.*, 2004), and after cytokine treatment (Wang *et al.*, 2005), increased numbers of EGFP-claudin-1-containing vesicles were not identified after LatA treatment. Moreover, the newly formed mRFP1-occludin intracellular pools did not colocalize with intracellular foci of EGFP-claudin-1 that were present with or without LatA treatment. Thus, it seems that the EGFP-claudin-1 redistribution observed represents a late event that occurs after the bulk of TER loss and is not associated with occludin internalization. Although these data cannot exclude changes in claudin-1 distribution or biochemical interactions that may accompany LatA-induced loss of barrier function, they do show that changes in claudin-1 distribution detectable by fluorescence microscopy do not accompany such TER loss.

One recent study has suggested that immature adherens junctions can be disassembled after latrunculin treatment (Ivanov *et al.*, 2005). To determine whether the loss of TER after LatA treatment could be due to loss of adherens junctions, E-cadherin and occludin were imaged simultaneously in immunostained monolayers. At 20 min after LatA addition, when TER loss was complete, occludin was largely removed from the TJ, whereas the distribution of E-cadherin was unaffected (Figure 4C). Thus, LatA treatment does not cause gross disassembly of adherens junctions in these monolayers under the conditions studied here.

Disruption of Epithelial Barrier Function by LatA Requires Membrane Traffic

The data show that, along with decreased F-actin content, the most prominent early change that accompanies LatA-induced loss of barrier function is the endocytic removal of occludin from the TJ. To test the role of endocytosis in LatA-induced TER loss, we blocked membrane traffic by reducing temperature. Reducing temperature from 32 to 18°C did not affect LatA-induced loss of barrier function. In contrast, LatA-induced TER loss was completely prevented at ≤14°C (Figure 5A). Similar results were obtained with nontransfected and transfected MDCK monolayers, verifying that this was not an artifact of fusion protein expression. The protective effect was also not due to inhibition of actin depolymerization at 14°C (Figure 5A). This abrupt blockade of LatA-induced TER loss at 14°C suggests that the protective effect is due to inhibition of membrane traffic, rather than effects on protein–protein interactions or enzymatic activity. To determine whether cooling to 14°C also prevented LatA-induced internalization of occludin, we studied monolayers expressing EGFP-β-actin and mRFP1-occludin. At 14°C, LatA addition did not cause redistribution or endocytosis of mRFP1-occludin (Figure 5B and Supplemental Movie S6). Thus, the LatA-dependent actin depolymerization is dissociated from effects of LatA on TER and occludin internalization at 14°C. These data suggest that endocytosis may be an important step in LatA-induced disruption of TJ barrier function.

To further test the dependence of LatA-induced TER loss on endocytosis, vesicular traffic was inhibited at 37°C using hypertonic media. This treatment inhibits multiple pathways of vesicular traffic, including transport from the *trans*-Golgi network to the plasma membrane, endocytosis, and retrograde transport of plasma membrane proteins into the
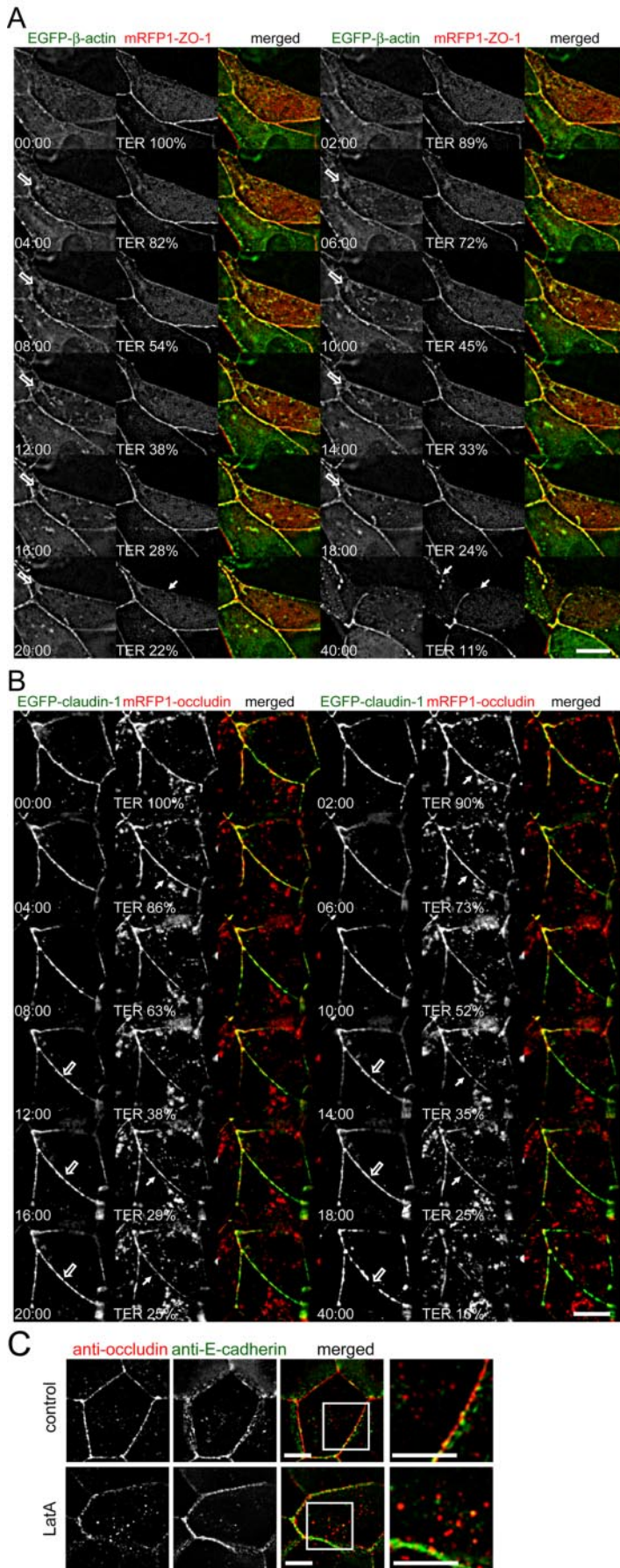
Figure 4. LatA-induced TER loss does not correlate with redistribution of ZO-1, claudin-1, or E-cadherin. (A) Confluent monolayers stably expressing EGFP-β-actin (left) and mRFP1-ZO-1 (middle) were imaged as z-stacks at 1-min intervals for 40 min after addition of 0.5 μM LatA. A single z-plane at the level of the TJ is shown. Time after LatA addition and TER, normalized to TER before LatA addition, are shown in each frame. Open arrows show aggregation and fusion of actin rich regions in apical surface. Solid arrows show changes of mRFP1-ZO-1 fluorescent intensity along the TJ. Bar, 20 μm. (B) Confluent monolayers stably expressing EGFP-claudin-1 (left) and mRFP1-occludin (middle) were imaged as z-stacks at 1-min intervals for 40 min after addition of 0.5 μM LatA. A single z-plane at the level of the TJ is shown. Time after LatA addition and TER, normalized to TER before LatA addition, are shown in each frame. Open arrows show changes in EGFP-claudin-1 fluorescence intensity along the TJ after LatA addition. These are not apparent until 12 min after LatA addition, when TER has already fallen by 62%. Solid arrows show changes of mRFP1-occludin fluorescent intensity along the TJ and formation of mRFP1-occludin containing vesicles. Bar, 20 μm. (C) MDCK monolayers not treated (top) or treated with 0.5 μM LatA (bottom) for 20 min were fixed with −20°C methanol/BS³ and stained for occludin (left) and E-cadherin (middle). Although the distribution of occludin is disrupted by LatA treatment, that of E-cadherin is not (merged images). This is confirmed at higher magnification (far right). Bars, 5 μm.
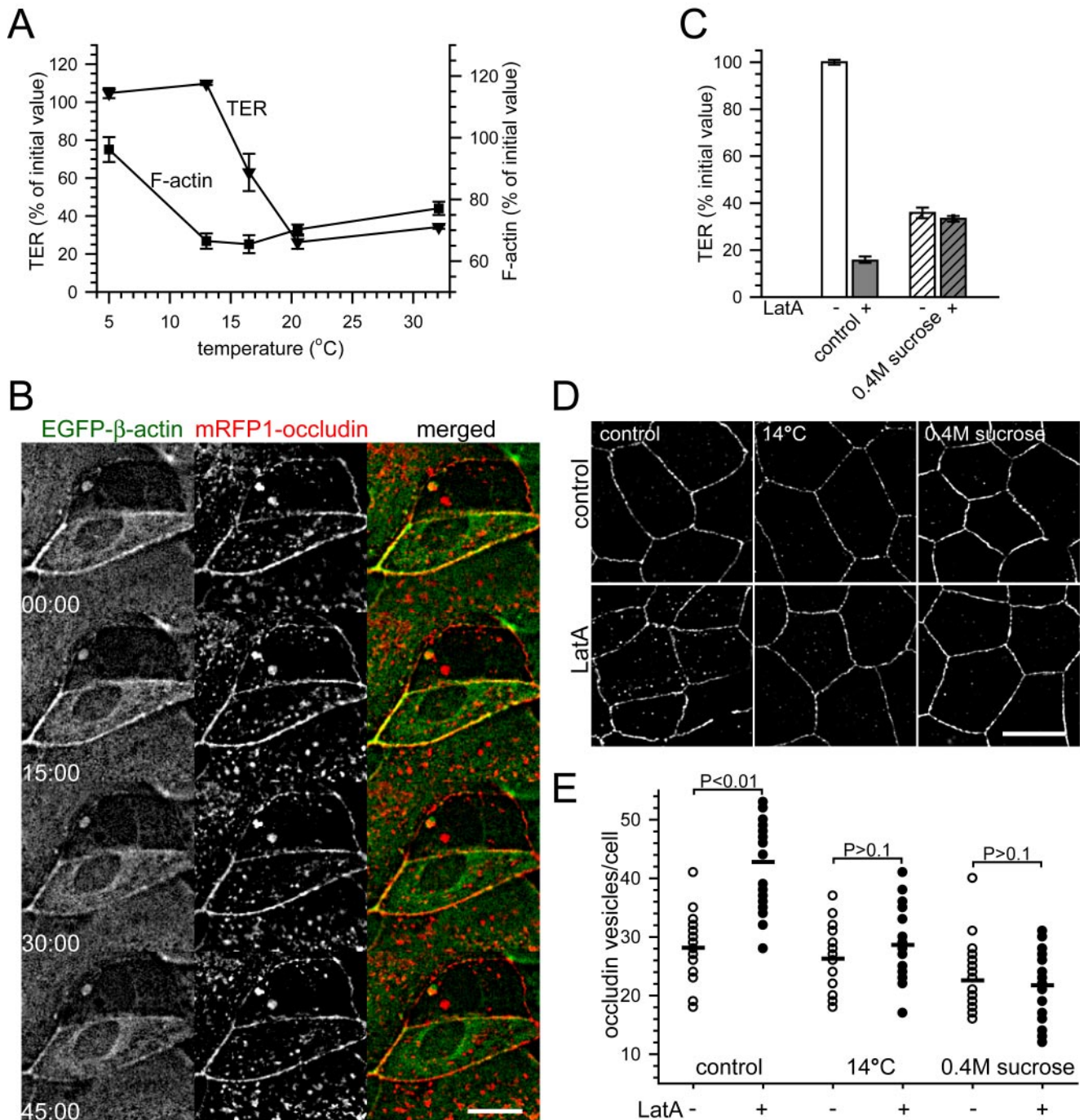
Figure 5. LatA-induced TER loss and occludin redistribution require membrane traffic. (A) MDCK monolayers were incubated at indicated temperature for 30 min before addition of 0.5 μM LatA. Because reduced temperature elevated TER, values 30 min after LatA addition are normalized to those before LatA addition. (B) MDCK monolayers expressing EGFP-β-actin (left) and mRFP1-occludin (middle) incubated at 14°C were imaged as z-stacks at 1-min intervals for 40 min after addition of 0.5 μM LatA. A single z-plane at the level of the TJ is shown. Time after LatA addition is shown in each frame. In contrast to 37°C, LatA did not induce occludin internalization at 14°C. However, actin was lost from the TJ. This can be best appreciated in the merged image where, due to loss of EGFP-β-actin, the TJ changes from yellow to red. Bar, 20 μm. (C) Monolayers were incubated in HBSS with 0.4 M sucrose for 1 h before addition of LatA. TER is shown 30 min after addition of LatA. Incubation in HBSS with 0.4 M sucrose decreased TER to 36 ± 2.3% of control, but LatA addition did not cause further TER loss. (D) MDCK monolayers were equilibrated in 37°C HBSS, 14°C HBSS, or 37°C HBSS with 0.4 M sucrose for 1 h and then treated without or with 0.5 μM LatA for 30 min under the same conditions. Monolayers were fixed with −20°C methanol/BS[3] and stained using mouse anti-occludin antibody. Disruption of occludin at the TJ and increased numbers of occludin-containing vesicles are apparent after LatA treatment. As in the live cell imaging (B), incubation at 14°C prevents accumulation of occludin-containing vesicles. Incubation in HBSS with 0.4 M sucrose also prevents accumulation of occludin-containing vesicles. Bar, 10 μm. (E) Morphometric analysis of occludin internalization. Each data set shows individual numbers of occludin vesicles per cell for 20 representative cells and the mean number of occludin vesicles per cell.
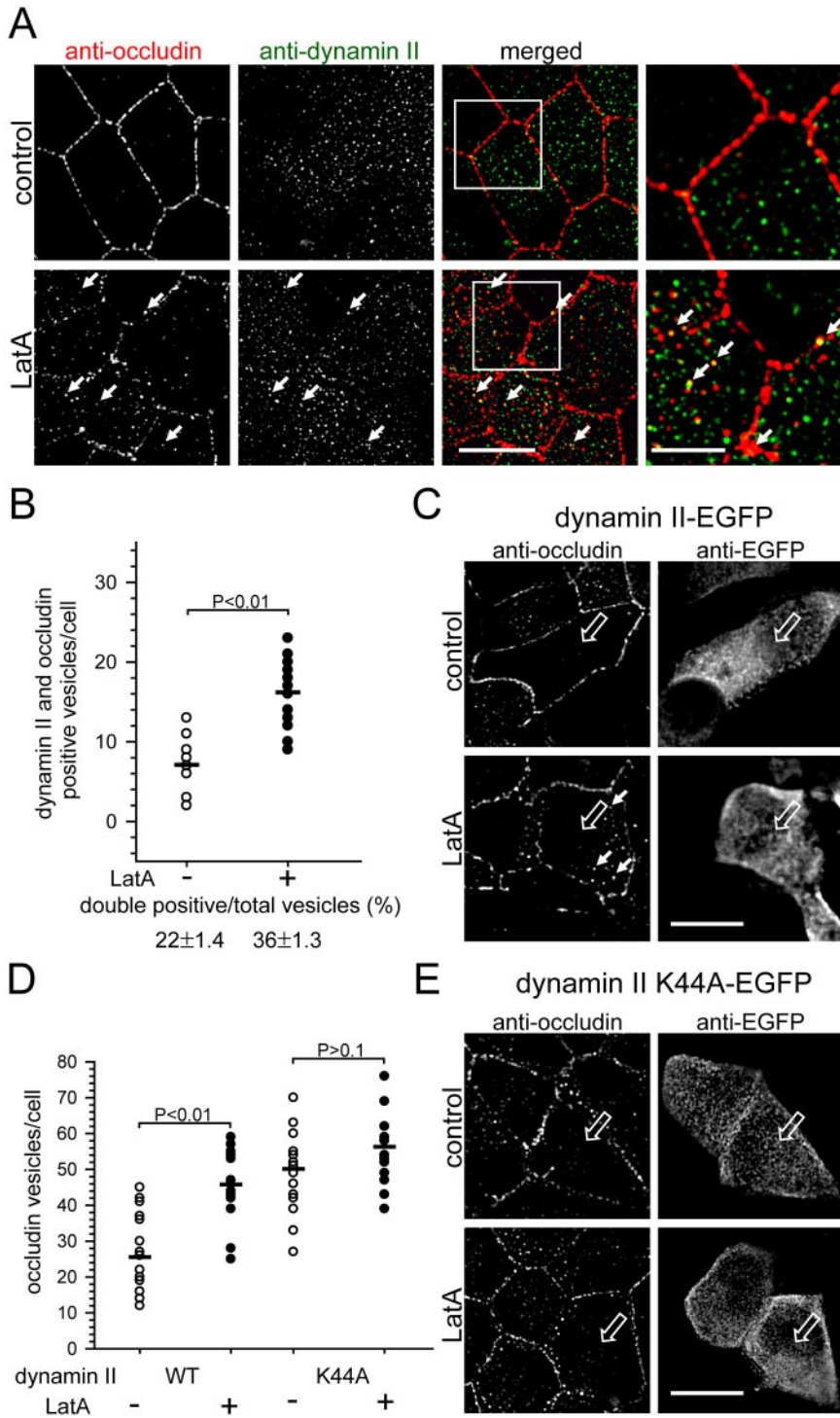
Figure 6. Occludin is internalized through a dynamin-II dependent pathway. (A) MDCK monolayers not treated (top) or treated with 0.5 μM LatA (bottom) for 30 min were fixed with $-20°$C methanol/BS^3 and stained for occludin (left) and dynamin II (middle). Increased colocalization is apparent after LatA treatment (merged images, arrows). Bar, 10 μm. Colocalization is more readily seen at higher magnification (far right). Bar, 5 μm. (B) Morphometric analysis of occludin and dynamin II colocalization. Each data set shows individual numbers of vesicles that label for both occludin and dynamin II per cell for 20 representative cells and the mean number of such vesicles per cell. The percentage of occludin vesicles that contain dynamin II is shown below each data set. (C) MDCK monolayers were transiently transfected with dynamin II-EGFP and incubated without or with 0.5 μM LatA for 30 min. After fixation with $-20°$C methanol/BS^3 monolayers were stained for occludin (left) and EGFP (right). Transfected cells (open arrows) were identified by the presence of EGFP. Cells expressing dynamin II-EGFP internalize occludin after LatA treatment similarly to nontransfected cells. Arrows show accumulation of occludin containing vesicles in dynamin II-EGFP-transfected cell after LatA treatment. Bar, 10 μm. (D) Morphometric analysis of occludin internalization. Each data set shows individual numbers of occludin vesicles per cell for 20 representative cells and the mean number of occludin vesicles per cell. (E) MDCK monolayers were transiently transfected with dynamin II K44A-EGFP and incubated without or with 0.5 μM LatA for 30 min. After fixation with $-20°$C methanol/BS^3 monolayers were stained for occludin (left) and EGFP (right). Transfected cells (open arrow) were identified by the presence of EGFP. Cells expressing dynamin II K44A-EGFP have increased numbers of occludin vesicles before LatA treatment but do not augment this number further after LatA treatment. Morphometric analysis of these conditions is shown in D. Bar, 10 μm.

Golgi complex (Docherty and Snider, 1991). Incubation of monolayers in media made hypertonic with 0.4 M sucrose caused TER to fall in the absence of LatA. However, no further loss of TER was induced by addition of LatA (Figure 5C), consistent with a requirement for vesicular transport in LatA-induced barrier dysfunction.

To perform quantitative analysis of the effects of lowered temperature and hypertonic buffer on occludin internalization, we sought to quantify intracellular occludin pools after LatA treatment in fixed preparations. However, the number

of occludin-containing intracellular vesicles detected in paraformaldehyde-fixed monolayers, either using anti-occludin immunolabeling or mRFP1-occludin fluorescence, was always less than the number detected by mRFP1-occludin fluorescence in live cells. We therefore considered the possibility that intracellular vesicles were damaged during paraformaldehyde fixation and subsequent processing. A protocol designed to prevent such damage by fixation in $-20°$C methanol followed by protein cross-linking (Hammond and Glick, 2000) successfully preserved intracellular
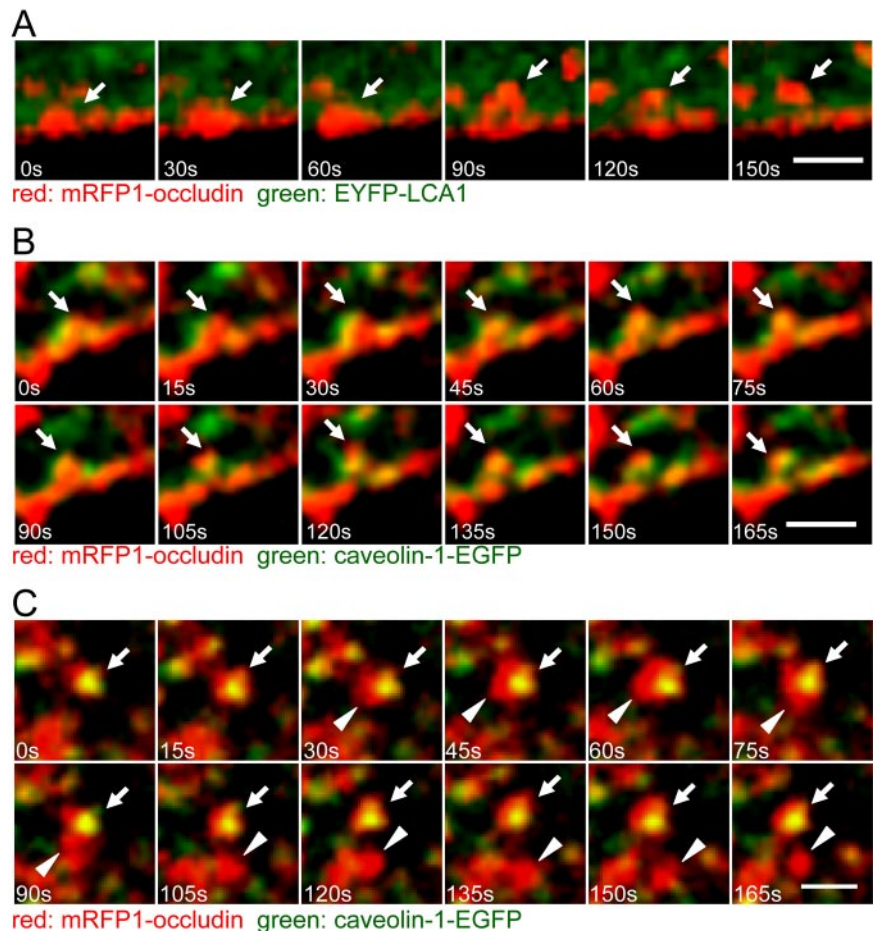
Figure 7. Occludin colocalizes with caveolin-1, but not clathrin light chain A1, during LatA-induced internalization. (A) MDCK monolayers expressing mRFP1-occludin and EYFP-clathrin light chain A1 were imaged after LatA treatment. The images, at 30-s intervals, show internalization of mRFP1-occludin (arrows) but no change in EYFP-clathrin light chain A1 distribution. Bar, 2 μm. (B) MDCK monolayers expressing mRFP1-occludin and caveolin-1-EGFP were imaged after LatA treatment. The images, at 15-s intervals, show cointernalization of mRFP1-occludin and caveolin-1-EGFP (arrows). Bar, 2 μm. (C) MDCK monolayers expressing mRFP1-occludin and caveolin-1-EGFP were imaged after LatA treatment. The images, at 15-s intervals, follow a vesicle internalized 10–15 min previously (arrows). mRFP1-occludin and caveolin-1-EGFP are initially colocalized within the vesicle. Some of the mRFP1-occludin then separates (arrowheads) from the caveolin-1-EGFP, first within what seems to be a single vesicle and later in a separate vesicle (arrowheads) that does not contain caveolin-1-EGFP. Bar, 2 μm.

occludin vesicles during fixation and subsequent immunostaining. This fixation protocol was used to assess intracellular occludin pools induced by LatA treatment in HBSS at 37 or 14°C or at 37°C in hypertonic buffer (Figure 5D). At 37°C, LatA treatment induced the accumulation of intracellular occludin-containing vesicles in fixed cells in a manner identical to that seen during live cell imaging, with an increase from 28 ± 1.2 to 43 ± 1.6 vesicles per cell (Figure 5, D and E; $p < 0.01$). In monolayers cooled to 14°C, LatA did not cause an increase in occludin-containing intracellular vesicles (Figure 5, D and E). Similarly, LatA did not cause occludin internalization in monolayers incubated in hypertonic buffer (Figure 5, D and E). Thus, LatA-induced TER loss and occludin internalization were both blocked when membrane traffic was inhibited at 14°C or with hypertonic media. These data show that LatA-induced TJ disruption requires membrane traffic that correlates with occludin internalization.

Occludin Is Internalized by a Dynamin II-dependent Process

To further understand the process by which occludin is internalized, potential pathways of occludin endocytosis were evaluated. Dynamin II plays an important role in caveolae- and clathrin-mediated endocytosis from basolateral membranes (van der Bliek *et al.*, 1993; Altschuler *et al.*, 1998; Oh *et al.*, 1998). In control monolayers, 6.8 ± 0.6 vesicles per cell labeled for both occludin and dynamin II. This represented $22 \pm 1.4\%$ of the 31 ± 1.7 occludin-containing

vesicles present in each cell. LatA treatment increased the number of occludin-containing vesicles that also contained dynamin II to 16 ± 0.9 per cell ($p < 0.01$), or $36 \pm 1.3\%$ of all occludin-containing vesicles (Figure 6, A and B). Dynamin II localization at the TJ also was occasionally seen in LatA-treated cells, but not in the absence of LatA treatment. These data suggest that dynamin II may be involved in the occludin endocytosis that occurs after LatA treatment.

To directly test the role of dynamin II in occludin endocytosis, MDCK cells were transiently transfected with dynamin II-EGFP or dynamin II K44A-EGFP. The latter is a dominant negative dynamin II that lacks GTPase activity and blocks both caveolae- and clathrin-mediated endocytosis (van der Bliek *et al.*, 1993; Oh *et al.*, 1998). In cells expressing dynamin II-EGFP, occludin was delivered to the TJ normally (Figure 6C), and LatA treatment caused the number of intracellular occludin vesicles to increase from 27 ± 2.4 to 45 ± 2.2 per cell (Figure 6D; $p < 0.01$). Monolayers expressing dynamin II K44A-EGFP had a reduced baseline TER that was $71 \pm 3\%$ of those expressing dynamin II-EGFP. Dynamin II K44A-EGFP-expressing cells displayed discontinuous occludin staining at the TJ (Figure 6E), with decreased intensity of TJ occludin staining and increased occludin-containing intracellular vesicles to 48 ± 2.5 per cell in the absence of LatA treatment (Figure 6, D and E). These data suggest that dynamin II may be important for basal delivery and recycling of occludin. When cells expressing dynamin II K44A-EGFP were treated with LatA there was no significant increase in the number of occludin-containing
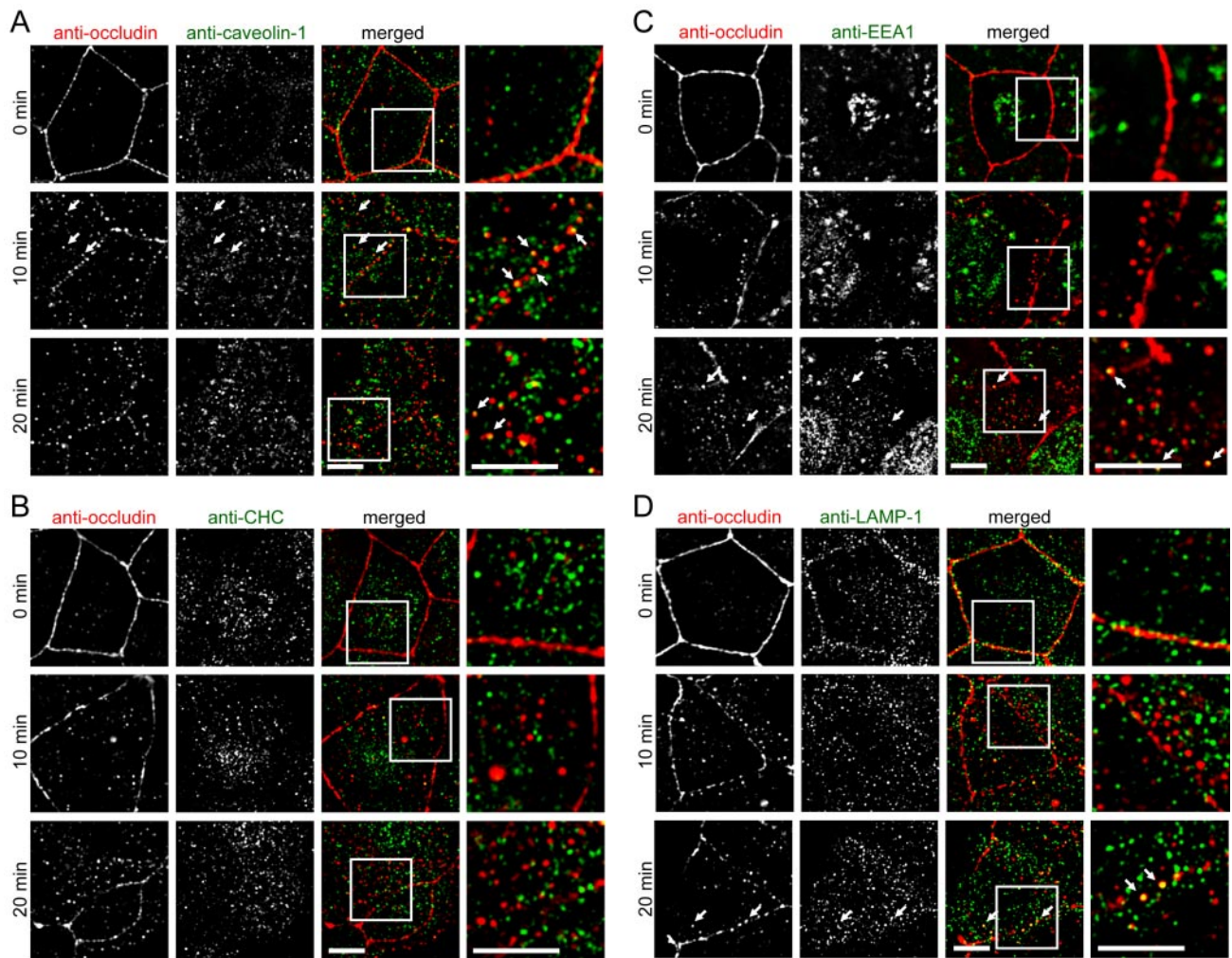
Figure 8. Occludin colocalizes primarily with caveolin-1, but not clathrin, EEA1, or LAMP-1, after LatA-induced internalization. (A) MDCK monolayers were cooled to 14°C, treated with 0.5 μM LatA for 30 min, and warmed to 37°C for indicated times before being fixed with −20°C methanol/BS³ and stained for occludin (left) and caveolin-1 (middle). Increased colocalization is apparent after warming, and is most prominent after 10 min (merged images, arrows). This colocalization is confirmed at higher magnification (far right). Bars: 5 μm. (B) MDCK monolayers were cooled to 14°C, treated with 0.5 μM LatA for 30 min, and warmed to 37°C for indicated times before being fixed with −20°C methanol/BS³ and stained for occludin (left) and clathrin heavy chain (middle). No significant colocalization is apparent before or after warming (merged images). This lack of colocalization is confirmed at higher magnification (far right). Bars, 5 μm. (C) MDCK monolayers were cooled to 14°C, treated with 0.5 μM LatA for 30 min, and warmed to 37°C for indicated times before being fixed with −20°C methanol/BS³ and stained for occludin (left) and EEA1 (middle). There is no significant colocalization before or 10 min after warming, but limited colocalization is present 20 min after warming (merged images, arrows). Colocalization is confirmed at higher magnification (far right). Bars, 5 μm. (D) MDCK monolayers were cooled to 14°C, treated with 0.5 μM LatA for 30 min, and warmed to 37°C for indicated times before being fixed with −20°C methanol/BS³ and stained for occludin (left) and LAMP-1 (middle). There is no significant colocalization before or 10 min after warming, but limited colocalization is present 20 min after warming (merged images, arrows). Colocalization is confirmed at higher magnification (far right). Bars, 5 μm.

intracellular vesicles (Figure 6, D and E). In contrast, expression of dominant negative dynamin I was unable to prevent occludin internalization (our unpublished observations). Because dominant negative dynamin I inhibits apical but not basolateral endocytic events in polarized epithelia (Altschuler *et al.*, 1998), this observation is consistent with the apparent origin of occludin-containing vesicles from the lower portion of the TJ adjacent to the border with the lateral membrane. Thus, these data demonstrate that LatA-induced occludin endocytosis occurs by a process that requires dynamin II function.

Occludin Is Internalized into Caveolin-1- but Not Clathrin-containing Vesicles

Dynamin II participates in both caveolae- and clathrin-mediated endocytosis (van der Bliek *et al.*, 1993; Oh *et al.*, 1998). Intracellular occludin has been identified in association with both caveolin-1 (Nusrat *et al.*, 2000b) and clathrin (Ivanov *et al.*, 2004). Thus, although the data show that dynamin II-mediated endocytosis is involved in LatA-induced occludin internalization and TER loss, they do not differentiate clathrin- and caveolae-mediated endocytic pathways. To evalu-
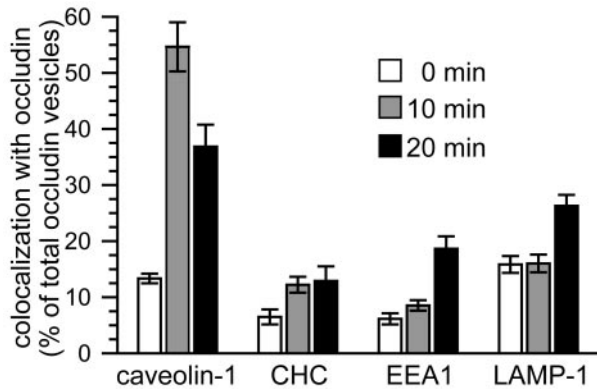
Figure 9. Occludin passes though a caveolin-1-containing compartment after LatA-induced internalization. Morphometric analysis of occludin colocalization with caveolin-1, clathrin heavy chain, EEA1, and LAMP-1 0, 10, and 20 min after warming. Each data set shows the fraction of vesicles that label for both occludin and the other indicated antigen for 20 representative cells in each condition.

ate the association of clathrin or caveolin with occludin during LatA-induced internalization, monolayers expressing mRFP1-occludin and either EYFP-clathrin light chain A1 or caveolin-1-EGFP were analyzed. mRFP1-occludin internalization was frequently observed in EYFP-clathrin light chain A1-expressing cells, but clathrin light chain A1 never colocalized with mRFP1-occludin during internalization (Figure 7A). In contrast, caveolin-1-EGFP colocalized with mRFP1-occludin in surface membrane invaginations and detaching vesicles in nearly all observed instances of LatA-induced occludin internalization (Figure 7B and Supplemental Movie S7). At later time points, some mRFP1-occludin could be seen to segregate away from caveolin-1-EGFP (Figure 7C and Supplemental Movie S8). Initially, a rim of occludin devoid of caveolin-1 was noticeable. Later, a separate vesicle containing occludin, but not caveolin-1, seemed to detach from the initial vesicle, resulting in two vesicles; one containing mRFP1-occludin and caveolin-1-EGFP and a second containing only mRFP1-occludin (Figure 7C).

To map these pathways quantitatively, it was necessary to synchronize occludin endocytosis. To accomplish this, we took advantage of the observation that occludin endocytosis did not occur at 14°C, although actin was effectively depolymerized at this temperature. Thus, monolayers were treated with LatA for 30 min at 14°C before being acutely warmed to 37°C. Before warming only 13% of occludin-containing vesicles were positive for caveolin-1 (Figures 8A and 9). Within 10 min after warming, this number increased to 55% (p < 0.001). However, this increase was transient, because 10 min later, at 20 min after warming, only 37% of occludin-containing vesicles were positive for caveolin-1 (Figures 8A and 9). These data are consistent with trafficking of internalized occludin through a caveolin-1-containing compartment.

A similar approach was used to evaluate the potential role of clathrin-mediated occludin endocytosis. In contrast to caveolin, LatA induced only a small increase in the number of occludin-containing vesicles positive for clathrin heavy chain, and this number was similar at both 10 and 20 min after warming (Figures 8B and 9). Trafficking of occludin to early and late endosomes also was assessed using EEA1 (Figure 8C) and LAMP-1 (Figure 8D), respectively, as markers of these compartments. In each case, increased labeling of

occludin-positive vesicles was only apparent 20 min after warming (Figure 9), at which time colocalization of caveolin-1 and occludin was decreasing. These data suggest that clathrin is not involved in the initial internalization of occludin and that this initial internalization does not involve EEA1-positive early endosomes. The observed separation of occludin from caveolin-1 and small increases in colocalization of occludin with EEA1 and LAMP-1 at later times raises the possibility that, like cholera toxin (Pelkmans et al., 2004), a fraction of occludin internalized through caveolae can be subsequently directed to other endocytic compartments.

LatA-induced Barrier Dysfunction Is Not Prevented by Inhibition of Clathrin-mediated Endocytosis or Macropinocytosis

To functionally define the role of clathrin-mediated endocytosis and macropinocytosis in LatA-induced TER loss, we assessed the effect of inhibitors of these pathways. Macropinocytosis was prevented with amiloride, which inhibits Na^+/H^+ exchange and blocks macropinocytosis without affecting clathrin-mediated endocytosis (West et al., 1989). LY294002 inhibits phosphoinositide 3-kinase and blocks maintenance, maturation, and translocation of macropinocytic vesicles (Araki et al., 1996; Murray et al., 2000). Neither of these drugs prevented LatA-induced barrier dysfunction (Figure 10A). Thus, although each of these drugs has additional effects unrelated to macropinocytosis, the failure of both to block LatA-induced barrier loss suggests that macropinocytosis does not play an important role in this process.

Chlorpromazine inhibits assembly of the clathrin adapter protein AP2, thereby blocking clathrin-mediated endocytosis (Petris et al., 2003). Although chlorpromazine increased TER to 175 ± 6.6% of control monolayers in the absence of LatA, it did not prevent LatA-induced TER loss (Figure 10B), suggesting that clathrin-mediated endocytosis is not involved in LatA-induced TJ disruption. Moreover, specific inhibition of clathrin-mediated endocytosis by expression of EGFP-Eps15Δ95-295 (Benmerah et al., 1999; Nichols et al., 2001) failed to block LatA-induced occludin internalization (Figure 10C). Thus, both pharmacological and dominant negative inhibition of clathrin-mediated endocytosis failed to prevent LatA-induced TER loss and occludin internalization, suggesting that this pathway is not essential for LatA-induced TJ disruption.

LatA-induced Barrier Dysfunction Is Prevented by Cholesterol Extraction

The data suggest that dynamin II-dependent occludin internalization is responsible for LatA-induced TER loss. The morphological and morphometric data suggest that this occludin internalization may occur via caveolae-mediated endocytosis. Caveolae-mediated endocytosis depends on the specialized lipid composition of caveolae. To functionally define the role of caveolae-mediated endocytosis in LatA-induced TER loss, we extracted membrane cholesterol using either MBCD or filipin III, both of which have been shown to block caveolae-mediated endocytosis (Pike and Casey, 2002; Shigematsu et al., 2003). MBCD and filipin III caused TER to decrease by 12 ± 0.6 and 25 ± 0.4%, respectively, consistent with a previous report (Francis et al., 1999). However, further TER decreases were not induced by LatA in MBCD- or filipin III-treated monolayers (Figure 11A). Repletion of cholesterol restored the sensitivity of barrier function to LatA treatment, confirming that the effect of MBCD was due to cholesterol extraction (Figure 11B). Morphological analysis confirmed that MBCD prevented LatA-induced occludin in-
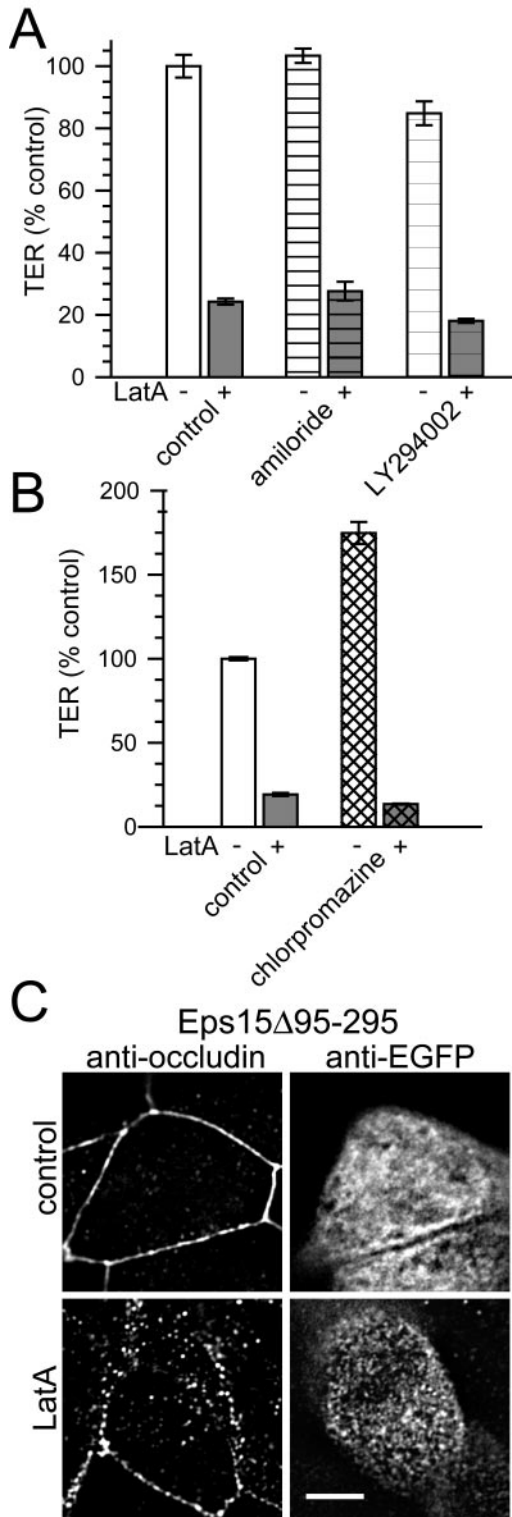
ternalization and that cholesterol repletion restored LatA-induced occludin internalization (Figure 11C). Moreover, morphometric analysis showed that although MBCD treatment alone caused the number of occludin-containing vesicles to increase slightly, from 28 ± 1.2 to 33 ± 1.7 vesicles per cell, there was no further increase upon LatA addition (Figure 11D). Thus, disruption of caveolae-mediated endocytosis prevents both LatA-induced barrier dysfunction and occludin internalization. Therefore, the functional and morphological data both indicate a critical role for caveolae-mediated endocytosis of TJ components, including occludin, in LatA-induced barrier disruption.

DISCUSSION

An essential function of epithelia is to form barriers. The TJ seals the paracellular space, thereby defining the epithelial barrier. Although it is widely accepted that the TJ requires an intact network of perijunctional actin, the specific role of actin in maintenance of the TJ remains ill-defined. For example, although actin depolymerization results in marked disruption of TJ structure and function, the intermediates in this process are unknown. Because multiple TJ proteins, including occludin, ZO-1, ZO-2, and ZO-3 interact with F-actin directly, a disruption of protein interactions has long been considered to be the mechanism of TJ disruption after actin depolymerization. However, this has not been tested directly, and the roles of other processes, e.g., endocytosis, have not been considered. To better define the events that link the model stimulus of actin depolymerization to TJ disruption, we developed fluorescent fusion proteins of actin and TJ proteins and analyzed them using an apparatus that allowed simultaneous imaging and determination of barrier function. The advances in temporal resolution afforded by this approach allowed us to identify and characterize a previously unrecognized redistribution of the TJ protein occludin that correlates temporally and functionally with TJ disruption. We show that this occludin redistribution requires membrane traffic and occurs via dynamin II-dependent caveolae-mediated endocytosis.

We first sought to develop appropriate fluorescent TJ protein fusion constructs. We selected ZO-1, the first identified TJ plaque protein, occludin, the first identified TJ transmembrane protein, and claudin-1, one of the first two identified members of the claudin family of proteins, as representatives of three classes of TJ proteins, plaque proteins, nonclaudin transmembrane proteins, and claudins, respectively. Each protein was tagged at a site remote from regions known to participate in protein–protein interactions or to otherwise be involved in function. Stably transfected cell lines expressing the fusion proteins at levels similar to or less than the endogenous proteins were chosen for further analyses to avoid artifacts due to simple protein overexpression. These lines all developed normal epithelial barrier function and responded to LatA in a dose-dependent manner that was nearly identical to that of the parental line. Immunofluorescent analyses and subcellular fractionation

Figure 10. Neither macropinocytosis nor clathrin-mediated endocytosis are required for LatA-induced barrier dysfunction or occludin internalization. (A) Monolayers pretreated with amiloride or LY294002 were treated with 0.5 μM LatA. TER is shown 30 min after addition of LatA. Neither macropinocytosis inhibitor prevented TER loss after LatA addition. (B) Monolayers treated with chlorpromazine showed a marked TER increase relative to control monolayers without chlorpromazine treatment. However, treatment with chlorpromazine, which inhibits clathrin-mediated endocytosis, did not prevent TER loss after LatA addition. (C) MDCK monolayers

were transiently transfected with EGFP-EpsΔ95-295 and incubated without or with 0.5 μM LatA for 30 min. After fixation with $-20°$C methanol/BS^3 monolayers were stained for occludin (left) and EGFP (right). Transfected cells were identified by the presence of EGFP. Cells expressing EGFP-EpsΔ95-295 internalized occludin in a manner indistinguishable from nontransfected cells, e.g., Figure 4D, after LatA treatment. Bar, 5 μm.
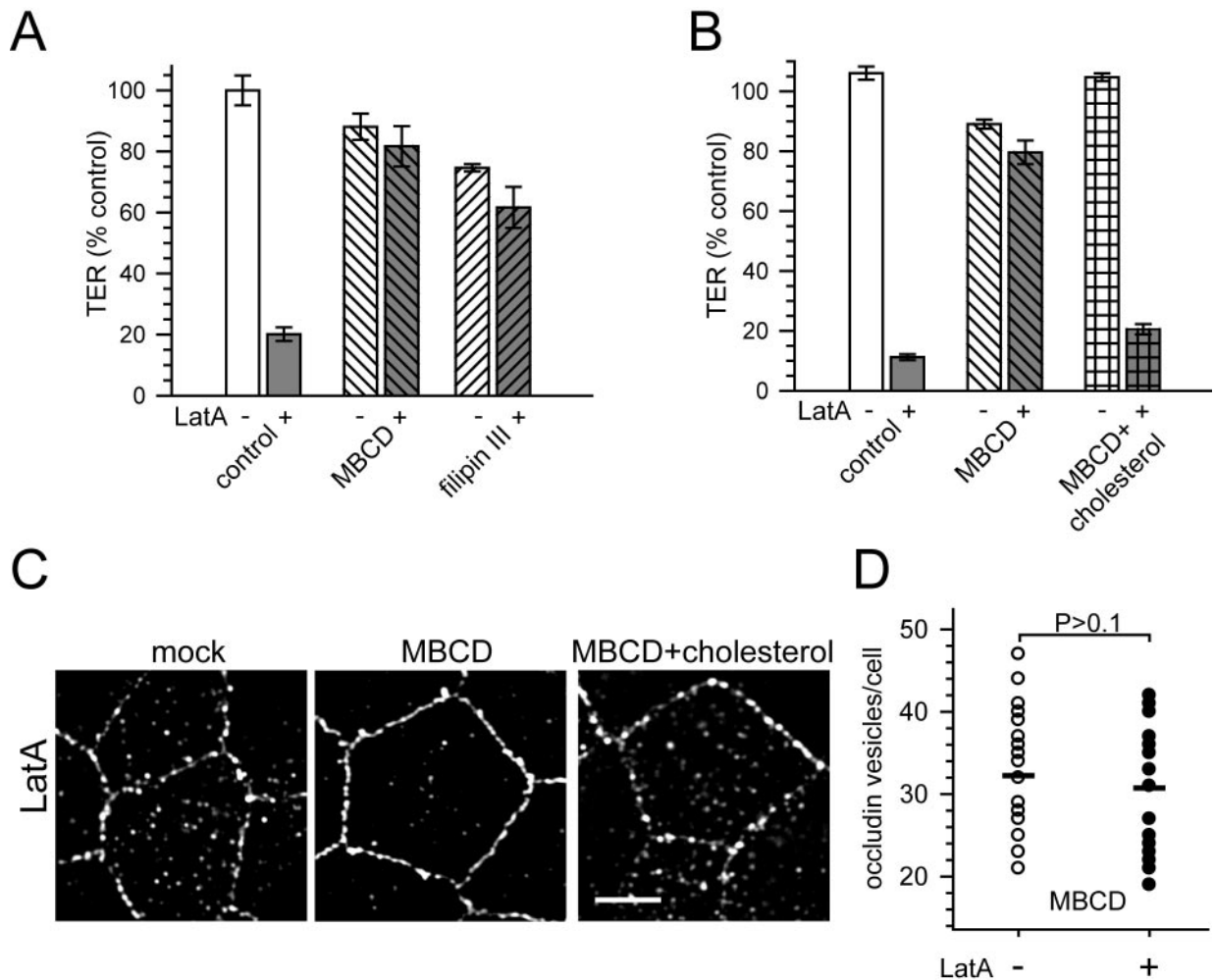
Figure 11. Caveolae-mediated endocytosis is required for LatA-induced barrier dysfunction and occludin internalization. (A) Treatment of monolayers with MBCD or filipin III caused a modest reduction in TER relative to control monolayers without MBCD or filipin III treatment. However, no further reduction in TER occurred after LatA addition. (B) MDCK monolayers were pretreated with MBCD and then treated with additional MBCD or MBCD-cholesterol complexes (MBCD+cholesterol) before treatment with 0.5 μM LatA for 30 min. As above, MBCD prevented LatA-induced TER loss, but sensitivity to LatA was restored by cholesterol repletion. (C) MDCK monolayers were pretreated with MBCD and then treated with additional MBCD or MBCD–cholesterol complexes (MBCD+cholesterol) before treatment with 0.5 μM LatA for 30 min. After fixation with -20°C methanol/BS^3 monolayers were stained for occludin. Consistent with the effects on TER, MBCD prevented LatA-induced occludin internalization, but sensitivity to LatA was restored by cholesterol repletion. Bar, 5 μm. (D) Morphometric analysis of occludin internalization in MBCD-treated monolayers. Each data set shows individual numbers of occludin vesicles per cell for 20 representative cells and the mean number of occludin vesicles per cell. MBCD prevented LatA-induced increases in occludin-containing vesicles.

studies showed that the fusion proteins were targeted identically to the corresponding endogenous TJ proteins. These fusion proteins also were redistributed by actin depolymerization in a manner similar to the endogenous proteins. Thus, the fusion proteins represent a suitable trace-label for tracking the movement of TJ proteins that does not significantly alter TJ morphology or barrier function.

Our initial studies of paraformaldehyde-fixed monolayers failed to identify morphological TJ disruption at early times after LatA addition, when barrier function was falling rapidly. Analysis of claudin-1 and ZO-1 fusion constructs also failed to show redistribution of these proteins that correlated with barrier loss. Subsequent studies using methanol fixation also failed to show redistribution of claudin-1, claudin-4, or ZO-1 until well after barrier loss had occurred. This should not be interpreted as indicating that these proteins are not involved in loss of barrier function, because changes

not detectable by fluorescence microscopy, including altered protein–protein interactions, may still play a role. However, the most striking morphological change that correlated precisely with loss of barrier function was the concentration of occludin at distinct sites with the TJ that were then internalized into vesicular cytoplasmic structures. This initially puzzled us, because these vesicles were not detected in our preliminary immunofluorescent studies using paraformaldehyde-fixed monolayers. The loss of these vesicles was resolved as a fixation artifact, because we found that vesicles containing endogenous occludin were detectable in LatA-treated monolayers fixed using a methanol-based protocol. Using this approach, we were able to confirm the occludin internalization seen in our live cell analyses.

Although occludin and claudins have been previously identified in intracellular vesicles, the mechanisms and functional significance of this localization remain uncertain. For

example, although a peculiar transcellular endocytosis of EGFP-claudin-3 has been reported, little is known of the mechanisms or functional consequences of this observation (Matsuda *et al.*, 2004). Occludin and claudin internalization has been reported in immunofluorescent studies of fixed cell preparations (Hopkins *et al.*, 2003; Ivanov *et al.*, 2004; Wang *et al.*, 2005), and data suggest that, after calcium chelation, occludin is internalized via a clathrin-mediated process (Ivanov *et al.*, 2004). In contrast, constitutive activation of rho, rac, and cdc42 using *Escherichia coli* cytotoxic necrotizing factor-1 has been associated with occludin internalization into caveolin-1-containing vesicles along with removal of ZO-1 and junction adhesion molecule-1 from the TJ (Hopkins *et al.*, 2003; Bruewer *et al.*, 2004). However, neither clathrin- nor caveolae-mediated occludin endocytosis was linked to changes in epithelial barrier function. Thus, although multiple mechanisms for internalization of occludin and other transmembrane TJ proteins have been reported, the relationship of these membrane trafficking events to TJ barrier function has not been explored previously. Given the striking temporal correlation we observed between occludin internalization and loss of barrier function, we sought to determine whether the membrane traffic this represented was essential to LatA-induced TJ barrier dysfunction.

To elucidate the role of membrane traffic in LatA-induced TJ barrier dysfunction, we used diverse inhibitors of membrane traffic. The data show that reduced temperature and hypertonicity prevent both the barrier dysfunction and occludin redistribution caused by LatA. Thus, these data are the first to show the absolute requirement for membrane traffic in TJ disruption induced by actin depolymerization. Given the range of membrane transport processes recently implicated in TJ protein internalization, we sought to identify the specific endocytic mechanisms that contribute to this TJ disruption. Based on lack of colocalization of internalized occludin with clathrin, the failure of the clathrin-mediated endocytosis inhibitor chlorpromazine to prevent LatA-induced barrier dysfunction, and the failure of Eps15Δ95-295 to prevent occludin internalization, we conclude that clathrin-mediated endocytosis is not critical to LatA-induced TJ disruption and occludin redistribution. Similarly, two separate inhibitors of fluid-phase macropinocytosis, amiloride and LY294002, were unable to prevent LatA-induced barrier dysfunction. We therefore also excluded macropinocytosis as a mechanism of TJ protein internalization and barrier dysfunction after actin depolymerization.

In contrast to clathrin-mediated endocytosis and macropinocytosis, several pieces of data point to caveolae-mediated endocytosis as the mechanism of occludin internalization in this process. First, extraction of plasma membrane cholesterol, which disrupts caveolae, prevented both barrier dysfunction and occludin redistribution after actin depolymerization. Second, both high-frequency imaging and morphometric analyses show that internalized occludin colocalizes with caveolin-1. Third, internalized occludin also colocalized with dynamin II and occludin internalization depended on dynamin II function, because dominant negative dynamin II prevented LatA-induced occludin internalization. Thus, although caveolae have not been reported within TJs, we conclude that similar caveolin- and dynamin II-dependent events are required for internalization of TJ proteins. This is also consistent with the observations that TJ proteins are present in detergent-resistant glycolipid- and cholesterol-rich membrane fractions (Nusrat *et al.*, 2000b) and that aggressive cholesterol extraction, using higher MBCD doses than those used here, disrupts barrier function (Francis *et al.*, 1999).

Thus, the data provide an alternative, although not mutually exclusive, explanation to the assumption that disruption of the direct binding interactions between TJ proteins and actin filaments explains the effects of actin depolymerization on barrier function. The data suggest that actin depolymerization triggers internalization of cholesterol-rich membranes, leading to TJ disruption. This is consistent with reports that cytochalasin D treatment increases lateral mobility of caveolin-1 and causes caveolae clustering (Thomsen *et al.*, 2002) and that SV40 virus binding induces transient actin depolymerization and dynamin-II recruitment that are necessary for formation of caveolae-derived endocytic vesicles (Pelkmans *et al.*, 2001, 2002). The phenomenon of clustering at the plasma membrane also may be related to the clustered occludin distribution and reduced barrier function we observed in dynamin II K44A-expressing monolayers. Based on the data presented here, one could hypothesize that depolymerization of actin allows increased lateral mobility of occludin, resulting in occludin clustering within TJ subdomains adjacent to lateral membrane. These regions then become the sites at which caveolae-mediated occludin internalization occurs using the endocytic machinery specialized for basolateral membrane domains. Although the data using a broad spectrum of inhibitors suggest that it is this process of endocytosis that causes loss of TJ barrier function, we cannot entirely exclude the possibility that barrier function is also compromised as occludin diffuses toward the lateral membrane.

In summary, these data show the critical role of membrane traffic in the functional and structural TJ disruption that is induced by actin depolymerization. Moreover, the data suggest that this membrane traffic is required for caveolae- and dynamin-mediated endocytosis of TJ components, including occludin. Thus, these data provide new understanding of the 25-year-old observation that actin depolymerization causes structural and functional TJ disruption. Moreover, although LatA-induced actin depolymerization is an artificial stimulus, it is possible that the mechanisms defined here are involved in the actomyosin-dependent TJ regulation that occurs throughout physiological and pathophysiological processes (Turner, 2000; Clayburgh *et al.*, 2004).

REFERENCES

Altschuler, Y., Barbas, S. M., Terlecky, L. J., Tang, K., Hardy, S., Mostov, K. E., and Schmid, S. L. (1998). Redundant and distinct functions for dynamin-1 and dynamin-2 isoforms. J. Cell Biol. *143*, 1871–1881.

Araki, N., Johnson, M. T., and Swanson, J. A. (1996). A role for phosphoinositide 3-kinase in the completion of macropinocytosis and phagocytosis by macrophages. J. Cell Biol. *135*, 1249–1260.

Bazzoni, G., Martinez-Estrada, O. M., Orsenigo, F., Cordenonsi, M., Citi, S., and Dejana, E. (2000). Interaction of junctional adhesion molecule with the tight junction components ZO-1, cingulin, and occludin. J. Biol. Chem. *275*, 20520–20526.

Benmerah, A., Bayrou, M., Cerf-Bensussan, N., and Dautry-Varsat, A. (1999). Inhibition of clathrin-coated pit assembly by an Eps15 mutant. J. Cell Sci. *112*, 1303–1311.

Bentzel, C. J., Hainau, B., Ho, S., Hui, S. W., Edelman, A., Anagnostopoulos, T., and Benedetti, E. L. (1980). Cytoplasmic regulation of tight-junction permeability: effect of plant cytokinins. Am. J. Physiol. *239*, C75–C89.

Bruewer, M., Hopkins, A. M., Hobert, M. E., Nusrat, A., and Madara, J. L. (2004). RhoA, Rac1, Cdc42 exert distinct effects on the epithelial barrier via selective structural and biochemical modulation of junctional proteins and F-actin. Am. J. Physiol. *287*, C327–C335.

Campbell, R. E., Tour, O., Palmer, A. E., Steinbach, P. A., Baird, G. S., Zacharias, D. A., and Tsien, R. Y. (2002). A monomeric red fluorescent protein. Proc. Natl. Acad. Sci. USA *99*, 7877–7882.

Chen, Y., Merzdorf, C., Paul, D. L., and Goodenough, D. A. (1997). COOH terminus of occludin is required for tight junction barrier function in early *Xenopus* embryos. J. Cell Biol. *138*, 891–899.

Choidas, A., Jungbluth, A., Sechi, A., Murphy, J., Ullrich, A., and Marriott, G. (1998). The suitability and application of a GFP-actin fusion protein for long-term imaging of the organization and dynamics of the cytoskeleton in mammalian cells. Eur. J. Cell Biol. *77*, 81–90.

Christian, A., Haynes, M., Phillips, M., and Rothblat, G. (1997). Use of cyclodextrins for manipulating cellular cholesterol content. J. Lipid Res. *38*, 2264–2272.

Citi, S., Sabanay, H., Jakes, R., Geiger, B., and Kendrick-Jones, J. (1988). Cingulin, a new peripheral component of tight junctions. Nature *333*, 272–275.

Clayburgh, D. R., Shen, L., and Turner, J. R. (2004). A porous defense: the leaky epithelial barrier in intestinal disease. Lab. Invest. *84*, 282–291.

Colegio, O. R., Van Itallie, C., Rahner, C., and Anderson, J. M. (2003). Claudin extracellular domains determine paracellular charge selectivity and resistance but not tight junction fibril architecture. Am. J. Physiol. *284*, C1346–C54.

Cooper, J. A. (1987). Effects of cytochalasin and phalloidin on actin. J. Cell Biol. *105*, 1473–1478.

Di, A., Nelson, D. J., Bindokas, V., Brown, M. E., Libunao, F., and Palfrey, H. C. (2003). Dynamin regulates focal exocytosis in phagocytosing macrophages. Mol. Biol. Cell *14*, 2016–2028.

Docherty, P. A., and Snider, M. D. (1991). Effects of hypertonic and sodium-free medium on transport of a membrane glycoprotein along the secretory pathway in cultured mammalian cells. J. Cell. Physiol. *146*, 34–42.

Francis, S. A., Kelly, J. M., McCormack, J., Rogers, R. A., Lai, J., Schneeberger, E. E., and Lynch, R. D. (1999). Rapid reduction of MDCK cell cholesterol by methyl-beta-cyclodextrin alters steady state transepithelial electrical resistance. Eur. J. Cell Biol. *78*, 473–484.

Furuse, M., Fujita, K., Hiiragi, T., Fujimoto, K., and Tsukita, S. (1998). Claudin-1 and -2, novel integral membrane proteins localizing at tight junctions with no sequence similarity to occludin. J. Cell Biol. *141*, 1539–1550.

Furuse, M., Hirase, T., Itoh, M., Nagafuchi, A., Yonemura, S., Tsukita, S., and Tsukita, S. (1993). Occludin: a novel integral membrane protein localizing at tight junctions. J. Cell Biol. *123*, 1777–1788.

Hammond, A. T., and Glick, B. S. (2000). Dynamics of transitional endoplasmic reticulum sites in vertebrate cells. Mol. Biol. Cell *11*, 3013–3030.

Haskins, J., Gu, L., Wittchen, E. S., Hibbard, J., and Stevenson, B. R. (1998). ZO-3, a novel member of the MAGUK protein family found at the tight junction, interacts with ZO-1 and occludin. J. Cell Biol. *141*, 199–208.

Hopkins, A. M., Walsh, S. V., Verkade, P., Boquet, P., and Nusrat, A. (2003). Constitutive activation of Rho proteins by CNF-1 influences tight junction structure and epithelial barrier function. J. Cell Sci. *116*, 725–742.

Ivanov, A. I., Hunt, D., Utech, M., Nusrat, A., and Parkos, C. A. (2005). Differential roles for actin polymerization and a myosin II motor in assembly of the epithelial apical junctional complex. Mol. Biol. Cell *16*, 2636–2650.

Ivanov, A. I., Nusrat, A., and Parkos, C. A. (2004). Endocytosis of epithelial apical junctional proteins by a clathrin-mediated pathway into a unique storage compartment. Mol. Biol. Cell *15*, 176–188.

Jesaitis, L. A., and Goodenough, D. A. (1994). Molecular characterization and tissue distribution of ZO-2, a tight junction protein homologous to ZO-1 and the *Drosophila* discs-large tumor suppressor protein. J. Cell Biol. *124*, 949–961.

MacLean-Fletcher, S., and Pollard, T. D. (1980). Mechanism of action of cytochalasin B on actin. Cell *20*, 329–341.

Madara, J. L. (1987). Intestinal absorptive cell tight junctions are linked to cytoskeleton. Am. J. Physiol. *253*, C171–C175.

Madara, J. L., Barenberg, D., and Carlson, S. (1986). Effects of cytochalasin D on occluding junctions of intestinal absorptive cells: further evidence that the cytoskeleton may influence paracellular permeability and junctional charge selectivity. J. Cell Biol. *102*, 2125–2136.

Martin-Padura, I., *et al.* (1998). Junctional adhesion molecule, a novel member of the immunoglobulin superfamily that distributes at intercellular junctions and modulates monocyte transmigration. J. Cell Biol. *142*, 117–127.

Massol, R. H., Larsen, J. E., Fujinaga, Y., Lencer, W. I., and Kirchhausen, T. (2004). Cholera toxin toxicity does not require functional Arf6- and dynamin-dependent endocytic pathways. Mol. Biol. Cell *15*, 3631–3641.

Matsuda, M., Kubo, A., Furuse, M., and Tsukita, S. (2004). A peculiar internalization of claudins, tight junction-specific adhesion molecules, during the intercellular movement of epithelial cells. J. Cell Sci. *117*, 1247–1257.

McCarthy, K. M., Skare, I. B., Stankewich, M. C., Furuse, M., Tsukita, S., Rogers, R. A., Lynch, R. D., and Schneeberger, E. E. (1996). Occludin is a functional component of the tight junction. J. Cell Sci. *109*, 2287–2298.

Meza, I., Sabanero, M., Stefani, E., and Cereijido, M. (1982). Occluding junctions in MDCK cells: modulation of transepithelial permeability by the cytoskeleton. J. Cell. Biochem. *18*, 407–421.

Morton, W. M., Ayscough, K. R., and McLaughlin, P. J. (2000). Latrunculin alters the actin-monomer subunit interface to prevent polymerization. Nat. Cell Biol. *2*, 376–378.

Murray, J., Wilson, L., and Kellie, S. (2000). Phosphatidylinositol-3′ kinase-dependent vesicle formation in macrophages in response to macrophage colony stimulating factor. J. Cell Sci. *113*, 337–348.

Nichols, B. J., Kenworthy, A. K., Polishchuk, R. S., Lodge, R., Roberts, T. H., Hirschberg, K., Phair, R. D., and Lippincott-Schwartz, J. (2001). Rapid cycling of lipid raft markers between the cell surface and Golgi complex. J. Cell Biol. *153*, 529–541.

Nusrat, A., Chen, J. A., Foley, C. S., Liang, T. W., Tom, J., Cromwell, M., Quan, C., and Mrsny, R. J. (2000a). The coiled-coil domain of occludin can act to organize structural and functional elements of the epithelial tight junction. J. Biol. Chem. *275*, 29816–29822.

Nusrat, A., Parkos, C. A., Verkade, P., Foley, C. S., Liang, T. W., Innis-Whitehouse, W., Eastburn, K. K., and Madara, J. L. (2000b). Tight junctions are membrane microdomains. J. Cell Sci. *113*, 1771–1781.

Oh, P., McIntosh, D. P., and Schnitzer, J. E. (1998). Dynamin at the neck of caveolae mediates their budding to form transport vesicles by GTP-driven fission from the plasma membrane of endothelium. J. Cell Biol. *141*, 101–114.

Pelkmans, L., Burli, T., Zerial, M., and Helenius, A. (2004). Caveolin-stabilized membrane domains as multifunctional transport and sorting devices in endocytic membrane traffic. Cell *118*, 767–780.

Pelkmans, L., Kartenbeck, J., and Helenius, A. (2001). Caveolar endocytosis of simian virus 40 reveals a new two-step vesicular-transport pathway to the ER. Nat. Cell Biol. *3*, 473–483.

Pelkmans, L., Puntener, D., and Helenius, A. (2002). Local actin polymerization and dynamin recruitment in SV40-induced internalization of caveolae. Science *296*, 535–539.

Peng, B. H., Lee, J. C., and Campbell, G. A. (2003). In vitro protein complex formation with cytoskeleton-anchoring domain of occludin identified by limited proteolysis. J. Biol. Chem. *278*, 49644–49651.

Petris, M. J., Smith, K., Lee, J., and Thiele, D. J. (2003). Copper-stimulated endocytosis and degradation of the human copper transporter, hCtr1. J. Biol. Chem. *278*, 9639–9646.

Pike, L. J., and Casey, L. (2002). Cholesterol levels modulate epidermal growth factor (EGF) receptor-mediated signaling by altering receptor function and trafficking. Biochemistry *41*, 10315–10322.

Riesen, F. K., Rothen-Rutishauser, B., and Wunderli-Allenspach, H. (2002). A ZO1-GFP fusion protein to study the dynamics of tight junctions in living cells. Histochem. Cell Biol. *117*, 307–315.

Ryeom, S. W., Paul, D., and Goodenough, D. A. (2000). Truncation mutants of the tight junction protein ZO-1 disrupt corneal epithelial cell morphology. Mol. Biol. Cell *11*, 1687–1696.

Saitou, M., Furuse, M., Sasaki, H., Schulzke, J. D., Fromm, M., Takano, H., Noda, T., and Tsukita, S. (2000). Complex phenotype of mice lacking occludin, a component of tight junction strands. Mol. Biol. Cell *11*, 4131–4142.

Sasaki, H., Matsui, C., Furuse, K., Mimori-Kiyosue, Y., Furuse, M., and Tsukita, S. (2003). Dynamic behavior of paired claudin strands within apposing plasma membranes. Proc. Natl. Acad. Sci. USA *100*, 3971–3976.

Shigematsu, S., Watson, R. T., Khan, A. H., and Pessin, J. E. (2003). The adipocyte plasma membrane caveolin functional/structural organization is necessary for the efficient endocytosis of GLUT4. J. Biol. Chem. *278*, 10683–10690.

Simon, D. B., *et al.* (1999). Paracellin-1, a renal tight junction protein required for paracellular Mg2+ resorption. Science *285*, 103–106.

Spector, I., Shochet, N. R., Blasberger, D., and Kashman, Y. (1989). Latruncu-lins–novel marine macrolides that disrupt microfilament organization and affect cell growth: I. Comparison with cytochalasin D. Cell Motil. Cytoskele-ton 13, 127–144.

Spector, I., Shochet, N. R., Kashman, Y., and Groweiss, A. (1983). Latruncu-lins: novel marine toxins that disrupt microfilament organization in cultured cells. Science 219, 493–495.

Stevenson, B. R., and Begg, D. A. (1994). Concentration-dependent effects of cytochalasin D on tight junctions and actin filaments in MDCK epithelial cells. J. Cell Sci. 107, 367–375.

Stevenson, B. R., Siciliano, J. D., Mooseker, M. S., and Goodenough, D. A. (1986). Identification of ZO-1: A high molecular weight polypeptide associ-ated with the tight junction (zonula occludens) in a variety of epithelia. J. Cell Biol. 103, 755–766.

Thomsen, P., Roepstorff, K., Stahlhut, M., and van Deurs, B. (2002). Caveolae are highly immobile plasma membrane microdomains, which are not in-volved in constitutive endocytic trafficking. Mol. Biol. Cell 13, 238–250.

Turner, J. R. (2000). 'Putting the squeeze' on the tight junction: understanding cytoskeletal regulation. Semin. Cell Dev. Biol. 11, 301–308.

Turner, J. R., Rill, B. K., Carlson, S. L., Carnes, D., Kerner, R., Mrsny, R. J., and Madara, J. L. (1997). Physiological regulation of epithelial tight junctions is

associated with myosin light-chain phosphorylation. Am. J. Physiol. 273, C1378–C1385.

Umeda, K., Matsui, T., Nakayama, M., Furuse, K., Sasaki, H., Furuse, M., and Tsukita, S. (2004). Establishment and characterization of cultured epithelial cells lacking expression of ZO-1. J. Biol. Chem. 279, 44785–44794.

van der Bliek, A. M., Redelmeier, T. E., Damke, H., Tisdale, E. J., Meyerowitz, E. M., and Schmid, S. L. (1993). Mutations in human dynamin block an intermediate stage in coated vesicle formation. J. Cell Biol. 122, 553–563.

Wang, F., Graham, W. V., Wang, Y., Witkowski, E. D., Schwarz, B. T., and Turner, J. R. (2005). IFNγ and TNFα synergize to induce intestinal epithelial barrier dysfunction by upregulating MLC kinase expression. Am. J. Pathol. 166, 409–419.

West, M. A., Bretscher, M. S., and Watts, C. (1989). Distinct endocytotic pathways in EGF-stimulated human carcinoma A431 cells. J. Cell Biol. 109, 2731–2739.

Wittchen, E. S., Haskins, J., and Stevenson, B. R. (1999). Protein interactions at the tight junction. Actin has multiple binding partners, and ZO-1 forms independent complexes with ZO-2 and ZO-3. J. Biol. Chem. 274, 35179–35185.

Zhao, H., Shiue, H., Palkon, S., Wang, Y., Cullinan, P., Burkhardt, J. K., Musch, M. W., Chang, E. B., and Turner, J. R. (2004). Ezrin regulates NHE3 translocation and activation after Na+-glucose cotransport. Proc. Natl. Acad. Sci. USA 101, 9485–9490.